

**Geometric factors of Polyethylene particles and their effect on
the local CD3-positive immune response in histological slice
images**

**Geometrische Faktoren von Polyethylenpartikel und ihr
Effekt auf die lokale CD3-positive Immunantwort von
histologischen Schnittbildern**

Master's Thesis im Fach Medizintechnik

vorgelegt
von

Lara-Maria Steffes Steffes

Geboren am 27.05.1992 in Fürth

Angefertigt am

Lehrstuhl für Mustererkennung (Informatik 5)
Department Informatik
Friedrich-Alexander-Universität Erlangen-Nürnberg.

Technische Betreuer: Prof. Dr.-Ing. habil. Andreas Maier, Dipl.-Ing. Marc Aubreville, Dr. med.
Stefan M. Sesselmann und Prof. Dr. med. V. Krenn

Beginn der Arbeit: 01.04.2017

Abgabe der Arbeit: 30.09.2017

Ich versichere, dass ich die Arbeit ohne fremde Hilfe und ohne Benutzung anderer als der angegebenen Quellen angefertigt habe und dass die Arbeit in gleicher oder ähnlicher Form noch keiner anderen Prüfungsbehörde vorgelegen hat und von dieser als Teil einer Prüfungsleistung angenommen wurde. Alle Ausführungen, die wörtlich oder sinngemäß übernommen wurden, sind als solche gekennzeichnet. Die Richtlinien des Lehrstuhls für Studien- und Diplomarbeiten habe ich gelesen und anerkannt, insbesondere die Regelung des Nutzungsrechts.

Erlangen, den 29. September 2017

Übersicht

Ziel dieser Arbeit war die Entwicklung eines schwellwertbasierten Algorithmus zur Verarbeitung von histopathologischen Schnitten periimplantärer Membranen explantierter Kunstgelenke. Die zur Verfügung gestellten Bilder beinhalteten sowohl Polyethylenpartikel (Abriebpartikel) als auch CD3-positive Lymphozyten. CD3-positiven Lymphozyten waren als kleine, vorwiegend runde, braune Bereiche erkennbar. Polyethylenpartikel kamen in verschiedenen Größen vor und waren sichtbar als Aufhellungen im Bild. Mikropartikuläres Polyethylen hat einen Durchmesser kleiner als $5 \mu m$ und supramakropartikuläres Polyethylen Durchmesser größer als $100 \mu m$ mit einem Maximalwert von etwa $2200 \mu m$. Macropartikuläres Polyethylen befindet sich von der Größe zwischen diesen. Insgesamt sind 100 RGB-Bilder, die anlässlich von 52 Revisionsoperationen auf Grund einer diagnostizierten aseptischen Lockerung des Knie- bzw. Hüftgelenks gewonnen worden sind, zur Verfügung gestellt worden. Auf Grund der Schwankungen der Farbwerte und Intensitäten sowohl zwischen verschiedenen und innerhalb einzelner Bildern, wurden zuerst mit Hilfe von Normalisierungsverfahren (Macenko- und Reinhardnormalisierung) die Farb- und Intensitätswerte der Polyethylenpartikel, bzw. der CD3-positiven Lymphozyten angepasst. Mit weiteren Verfahren und einer abschließenden Blobdetektion konnten verschiedene Merkmale, welche anschließend zur Klassifizierung der Polyethylenpartikel und der CD3-positiven Lymphozyten genutzt wurden, extrahiert werden. Die CD3-positiven Lymphozyten wurden in die drei Klassen wenig, moderat und hoch eingeteilt. Die makro- und supramakropolyethylen Partikel wurden gezählt und das mikropartikuläre Polyethylen wurde in die drei Klassen wenig, moderat und hoch eingeteilt. Für die Klassifikation wurden die drei Klassifikationsmethoden Naive Bayes, Random Forest und Support Vector Machine genutzt. Zusätzlich wurde eine Abstandsmessung zur Bestimmung der benachbarten CD3-positiven Zellen zu den makro- und supramakropartikulären Polyethylenen, bzw. zu den mikropartikulären Polyethylenen, vorgenommen. Es wurde geklärt in wie weit die Größe der Polyethylenpartikel einen Einfluss auf die Immunantwort hat. Als Entwicklungsumgebung wurde PyCharm der Firma JetBrains für die Programmiersprache Python 3 genutzt.

Abstract

Aim of this thesis was the development of an threshold-based algorithm for the segmentation of histological slice images. The provided images contained a CD3-positive immune/inflammatory response, which was visible as small, mostly circular, brown dots and polyethylene (PE) particles (abrasion particles), visible as bright regions in different sizes. Micro-polyethylene (MPE) particles have a length smaller than $5\ \mu m$, macro-polyethylene (MacroPE) a size between $5\ \mu m$ and $100\ \mu m$ and supramacro-polyethylene (SMPE) particles a length greater than $100\ \mu m$ and a maximal size of $2200\ \mu m$. Therefore, 100 RGB images of stain colored human tissue, which were obtained during 52 revision surgeries on the basis of a diagnosed aseptic loosening of the knee or hip joint, were provided. Due to the occurring varieties in color and intensity values of the available images, stain normalization was necessary. The methods proposed by Reinhard et al. and Macenko et al. yielded good results. With further preprocessing methods and a final blob detection, it was possible to find the locations, numbers, areas, etc. of the CD3-positive immune/inflammatory response and the polyethylene particles. In a next step, the CD3-positive cells were classified into the three classes, low, moderate and high immune/inflammatory response. The SMPE and MacroPE particles were grouped together and counted and the MPE particles were classified into low, moderate and high. Therefore, the three supervised classification methods naive Bayes (NB), random forest (RF) and support vector machine (SVM) were used. In addition to the classification, a distance measure for counting the adjacent CD3-positive cells with a maximal distance of $5\ \mu m$ around the MacroPE/SMPE particles and the MPE particles, were implemented. It was clarified in how far a connection between the number of the MPE and the occurring strength of the CD3-positive immune/inflammatory response exists. As development environment, PyCharm from JetBrains was used for the programming language Python 3.

Contents

1	Introduction	1
2	Related Work	3
3	Medical Background	5
3.0.1	Arthroplasty	6
3.0.2	CD3-positive immune/inflammatory response	8
3.0.3	Polyethylene particles	9
3.0.4	Processing of the tissue	10
4	Material and Methods	13
4.1	Material	13
4.2	Preprocessing Methods	14
4.2.1	Normalization	15
4.2.2	Color Deconvolution	19
4.2.3	Thresholding	23
4.2.4	Morphological operations	24
4.2.5	Blob detection	26
4.2.6	Preprocessing Pipeline	28
4.3	Classification Methods	29
4.3.1	Naive Bayes classifier	29
4.3.2	Support vector machines	30
4.3.3	Random Forest	30
4.3.4	Nearest Neighbor Classifier	31
4.4	Additional	32

5	Results and Discussion	35
5.1	Features	35
5.1.1	Features of CD3-positive immune/inflammatory response	35
5.1.2	Features of PE particles	37
5.2	Classification	39
5.2.1	Classification of CD3-positive immune/inflammatory response with Naive Bayes	39
5.2.2	Classification of CD3-positive immune/inflammatory response with Support Vector Machines	41
5.2.3	Classification of CD3-positive immune/inflammatory response with Random Forest	42
5.2.4	Classification of PE particles with Naive Bayes	43
5.2.5	Classification of MPE particles with Naive Bayes	44
5.2.6	Classification of MPE particles with Support Vector Machine	45
5.2.7	Classification of MPE particles with Random Forest	46
5.3	Relationships between PE particles and CD3-positive immune/inflammatory response	47
6	Conclusion	51
7	Summary	53
	List of Figures	57
	List of Tables	61
	Bibliography	63

Chapter 1

Introduction

In Germany, arthroplasty, especially hip and knee endoprosthesis, is one of the most successful surgical procedures. Nevertheless the lifespan of implants is limited, mostly caused by aseptic loosening. Material abrasion seems to be an important factor of the loosening process [Hop17]. It can impose the formation of a synovial-like interface membrane (SLIM) between the implant and the bone and therefore result in a loosening of the implant [Hop16]. Different abrasion materials, dependent on the used material of the sliding pair of the endoprosthesis, can be found in the SLIM. It has to be determined, how far the different sizes of polyethylene particles have an influence on the immune response and the loosening process. Because of the high time effort for medical experts to count every abrasion particle and CD3-positive cell manually and the associated error susceptibility, aim of this thesis is to detect the abrasion particles, in this case the polyethylene particles of different sizes, and the associated CD3-positive immune/inflammatory response with a semi-automatic threshold-based algorithm.

The thesis is structured as follows:

Chapter 2 focused on the the theoretical background. First, in the medical part, the different polyethylene particles and the CD3-positive immune/inflammatory response are introduced in detail. After that, the technical background, i.e. the used image processing and classification methods, is explained. In chapter 3 the theory about the used materials and methods is explained on the basis of suitable images. Additionally, a graphical user interface (GUI) was designed and implemented for loading single images and returning the number of CD3-positive cells, the number of MPE and MacroPE/SMPE particles as well as the number of CD3-positive cells with a maximal distance of $5\mu m$ around the MacroPE/SMPE particles, respectively the MPE particles, in the image. In chapter 4 the results are shown and discussed. Last but not least, a conclusion containing a outlook followed by a summary will be complete the work.

Chapter 2

Related Work

In 2015, a quantifier for a similar problem, the detection of CD15-cells, has already been developed by the company VmScope Berlin GmbH [Köl15]. A straightforward modification of this CD15-Quantifier to a CD3-Quantifier for detecting CD3-positive cells failed. In average, only one in four CD3-positive cells was detected. In cases of images with a low number of CD3-positive cells, the predicted number of cells was still acceptable, but in cases of a higher number of CD3-positive cells and corresponding cell clusters, the algorithm failed completely, as closely adjacent cells were often summarized to one. One year later, the company VmScope developed a new algorithm for a CD3-Quantifier with much better results in counting the number of CD3-positive cells. Nevertheless, there were great deviations, caused by the closely adjacent cells, which were still summarized to one cell [Hop16]. In Figure 2.1, the result of the CD3-Quantifier is shown. The purple lines show the problematic results for cell clusters.

General since 2014, the four normalization algorithms: Reinhard et al., Macenko et al., Khan

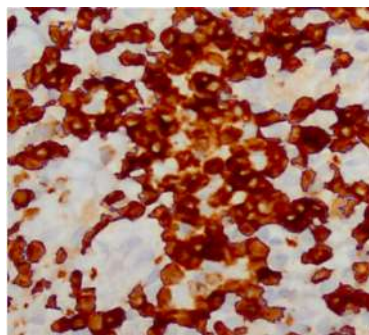


Figure 2.1: CD13-Quantifier for a histopathological slice image [Hop16]

et al. and a histogram specification, are part of the stain normalization toolbox of Warwick for the segmentation of eosin and hematoxylin (H&E) colored histology images [ToW15]. The

normalization method of Macenko et al. [Mac09] was presented in 2009 for the normalization of color and intensity variations of H&E stained slides of melanomas and nevi. Reinhard et al. [Rei01] presented already in 2001 a normalization method, which was originally for the processing of landscape photos. Khan et al. [Kha14] presents in 2014 a robust nonlinear mapping approach for the normalization of histopathology images. Additional to the normalization methods the stain normalization toolbox by Warwick contains a color deconvolution (CD) method, in which the RGB images are separated into three channels, corresponding to the stain concentrations. Already in 2001 a CD framework was represented by Ruifrok and Johnston [Rui01] for histopathology image analysis. The method was used in many applications, for example the quantification of immunohistochemical stains [Kha14].

Chapter 3

Medical Background

Material abrasion is suspected to be an important aspect for the loosening process [Hop17]. Thereby the abrasion particles promote the formation of a synovial-like-interface-membrane (SLIM) between bone and endoprostheses. After removing the endoprosthesis of the human body the SLIM can be prepared by immunohistochemistry. Thereby the histopathological classification and typing of the synovialis is performed according to the particle algorithm (see Figure 3.2) and the SLIM consensus classification (see Figure 3.1) [Hop16]. According to the consensus

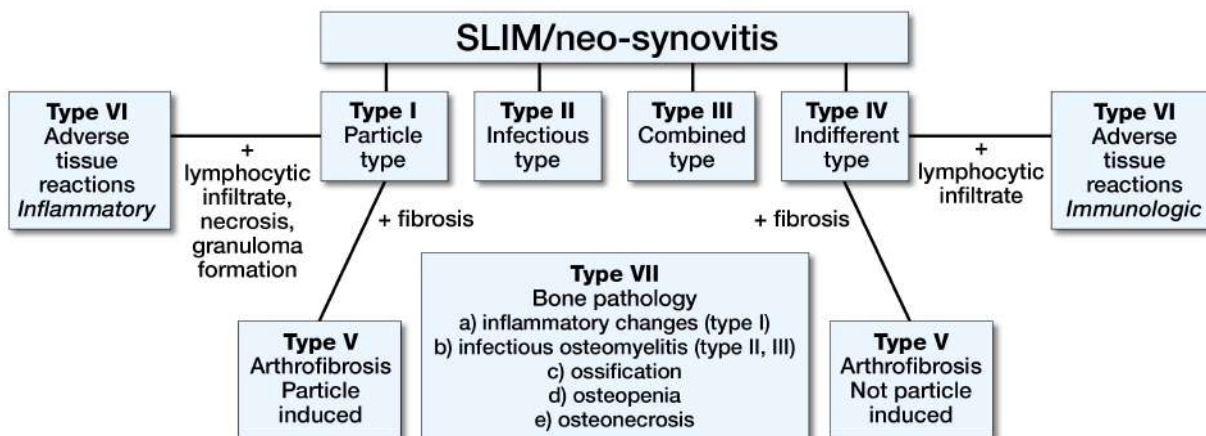


Figure 3.1: SLIM consensus classification of joint prosthesis pathology [Hop17]

classification the membrane can be divided into four types [Kre16]:

- type I = particle-induced type
- type II = infectious type
- Type III = combined type

- Type IV = indifferent type

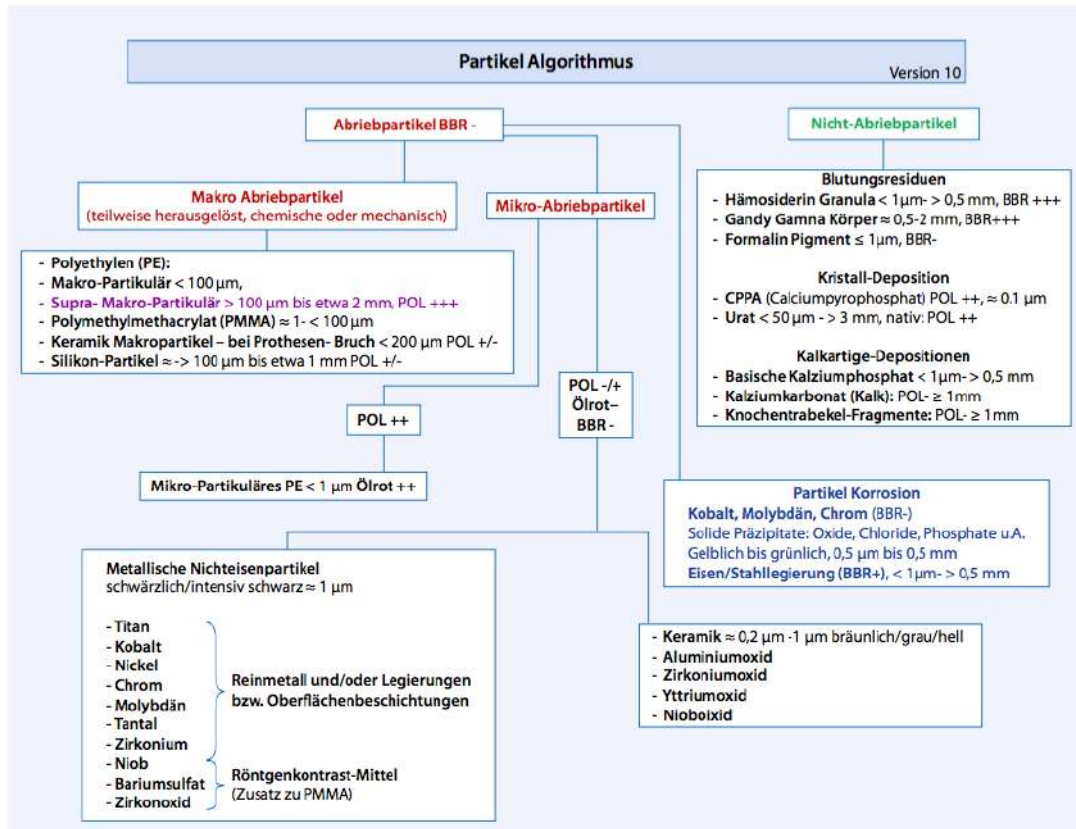


Figure 3.2: Particle algorithm [Kre16]

For this purpose, amongst other things, the concentration of the CD 3-positive immune/inflammatory response and the abrasion particles are determined [Hop16].

3.0.1 Arthroplasty

The implantation of a knee and hip joint endoprosthesis has long been a routine intervention. They are considered as therapy of choice as soon as the joint structure fails. In Germany, 15.7 million endoprostheses were produced in 2012. Since 2009, this number is nearly constant (see Figure 3.3). Permanently, new materials are developed and old materials are improved. About 200 companies are responsible for this considerable development [Hop16]. In Figure 3.4, two exemplary artificial endoprostheses are shown, on the left side a hip endoprosthesis with a metal-polyethylene sliding pairing and on the right side a knee endoprosthesis. In general, different material combinations for the sliding pairing are possible and must be weighed for each individual patient. In Figure 3.5,



Figure 3.3: Number of hip and knee implants in Germany [Lie16]

four of those combinations are shown. For the patient, artificial endoprosthesis offers a large gain in lost quality of life, as pain is reduced and lost mobility is restored. Often, sporting activities can be exercised again. Unfortunately, the life expectancy of endoprotheses is limited. After 10 years, approximately 5 percent of the patients already have primary complaints, they are no longer without pain. The cause of failure of an endoprosthesis can be multifactorial. The main unsolved problem is the loosening of the implant from the bone [Mül15]. Basically, there are two pathological mechanisms, which are responsible for the loosening of endoprotheses [Hop16].

Septic loosening

In the septic case, loosening is caused by early or late infections. Bacteria nest on the surface of the endoprosthesis and the body's defensive reaction leads to bone loss [Hop16].

Aseptic loosening

Aseptic loosening is significantly more frequent, spanning about 80 percent of the cases. At the beginning, there is a solid connection between endoprosthesis and bone, but after some time, the bone is increasingly replaced by a loosening or periprosthetic membrane (see Figure 3.6). This process of micro-movement causes strong pain for the patient [Hop16]. The process of loosening can not be undone. The endoprosthesis must be removed and replaced in a surgical procedure. After the removal of the endoprosthesis, the loosening membrane can be used for

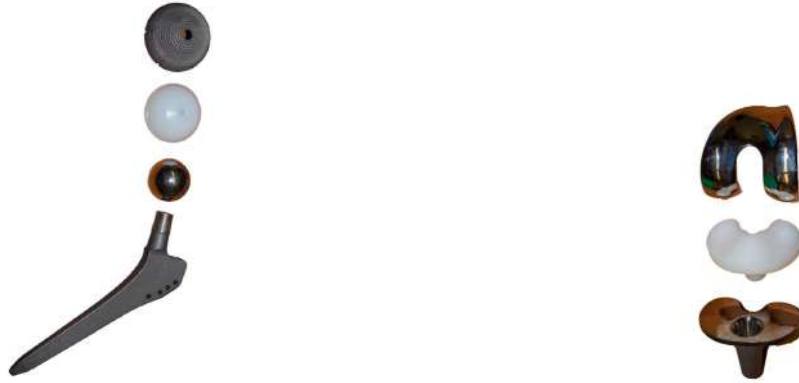


Figure 3.4: Left: Hip endoprosthesis with Me-PE sliding pairing; Right: Artificial knee endoprosthesis [Hop16]



Figure 3.5: Different material combinations for the sliding pair, from left to right: 1. metall-metall, 2. ceramics-ceramics, 3. ceramics-polyethylene, 4. metall-polyethylene [Hop16]

histopathological examination in order to clarify the cause. It is under discussion, whether a major cause of this membrane formation is a lymphocytic reaction to abrasion particles [Hop16] [Hop17]. Due to the size of the particles, removal of these particles via the lymphatic system is only possible in small quantities. As a result, there are accumulations in the periprosthetic soft tissues of these particles, which lead to a foreign body reaction. Especially T-lymphocytes are of great importance. By characteristic marker proteins, in this case CD3-positive, it is possible to make the cells immunohistochemically visible [Hop16].

3.0.2 CD3-positive immune/inflammatory response

CD3 protein complexes are located on the cell surfaces of the T-lymphocytes and are generally composed of four polypeptide chains. Phospholipidation of the CD3 complex leads to the activation of the T-lymphocytes, provoking the CD3-positive immune/inflammatory response [Hop16]. In Figure 3.7 the CD3-positive immune/inflammatory response is represented by the small dark circular dots. In the context of my work, the immune/inflammatory response should always be classified into the shown three classes, low, moderate and high.

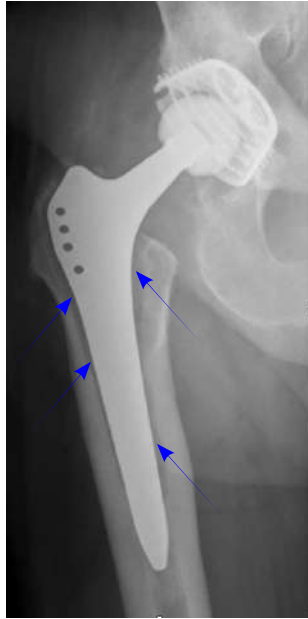


Figure 3.6: Aseptic loosening of a hip endoprosthesis; Formation of a SLIM (blue arrow) [Hop16]

3.0.3 Polyethylene particles

Polyethylene is mainly used for packaging and is the world's most important thermoplastic. In endoprosthesis two different kinds of thermoplasts are used: The particularly high molecular PE and a lower molecular PE.

To get the characteristic high level of particles the molecular chains are cross-linked by radioactive irradiation. Depending on the degree of cross-linking, different particle forms are available.

The major difference of these two kinds of PE in the endoprosthesis lies in the corresponding abrasion particles, which are e.g. caused by mechanical friction or impact. Higher crosslinked PE

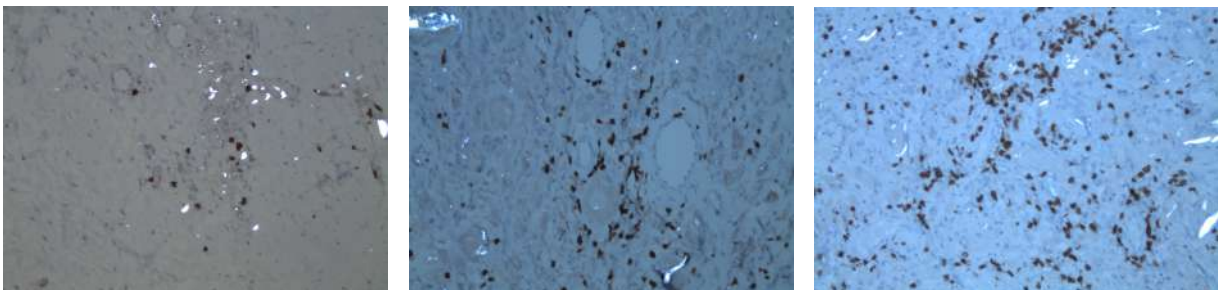


Figure 3.7: Histological images with a low, moderate and high CD3-positive immune/inflammatory response (from left to right)

leads mainly to small PE abrasion particles, the majority of non-crosslinked PE are taller sized PE particles [Hop16].

PE abrasion particles can be separated into micro-polyethylene (MPE), macro-polyethylene (MacroPE) and supra-macro-polyethylene (SMPE) [Kre16] with the size:

- MPE: $< 5 \mu m$
- MacroPE: $> 5 \mu m$ up to $100 \mu m$
- SMPE: $> 100 \mu m$ up to $2200 \mu m$

Due to the polarization-optical properties, PE abrasion particles are visible as white regions in the histological images [Hop16]. In Figure 3.8 these three different kinds of PE are shown. On the

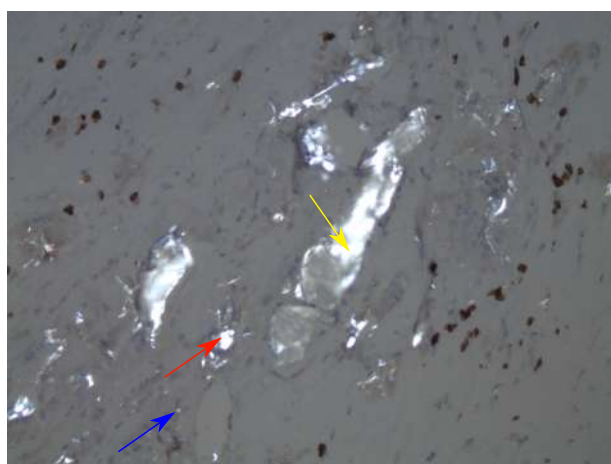


Figure 3.8: Histological image with SMPE (yellow arrow), MacroPE (red arrow) and MPE (blue arrow)

context of this thesis SMPE and MacroPE are grouped together and distinguished from MPE, which is divided into three classes: low, moderate and high immune/inflammatory response.

3.0.4 Processing of the tissue

A total of 100 preparations from 52 patients were used for this work. In all cases, aseptic loosening led to the removal of the implanted endoprotheses. A main condition was that no bacterial infection is present. This was proven hisopathologically and microbiologically.

The tissue was taken during the revision surgery of the loosened endoprotheses of the synovialis/SLIM. Then the tissue was sliced to a maximal thickness of 0.5 cm and buffered in formalin.

With different color reactions and techniques, it was possible to provoke the CD3-positive immune/inflammatory response and to visualize the polyethylene particles. On the one hand the CD3-positive lymphocytes were displayed immunohistochemically. Thereby solid-colored antibodies make certain cellular structures visible. The immunohistochemical presentation of CD3 lymphocytes was done by a fully automatic staining system. Hematoxylin was used for counter-staining, according to Harris [Hop16], resulting in a characteristic blue color. On the other hand, light microscopic morphological characteristics, polarized optical properties and enzymohistochemical characteristics in the oil red coloring and the Berliner-Blau reaction were used for the detection of the PE particles [Hop16] [Kre16].

Chapter 4

Material and Methods

In the following chapter, the available materials and the theory behind the used methods will be explained. For a better understanding, the methods will be applied on four different images with varying color and intensity. Additionally, a brief overview on the designed and implemented graphical user interface (GUI) for the medical team is finally given.

4.1 Material

100 images of a total of 100 prepared and colored tissue samples of 52 patients were available for this work. A main condition was that no bacterial infection is present. This was proven hisopathologically and microbiologically.

The 100 RGB images had a fix width of $594 \mu m$, corresponding to 2048 pixels. The most images have a height of 1536 pixels, in some cases a smaller height was available. Some of the images were available in 'JPEG' format, while the most images were available in 'PNG'.

For all images the strength of the CD3-positive immune/inflammatory response, the number of MacroPE/SMPE particles and the class of the MPE particles were available as reference. They were labeled by a medical expert.

For training and testing, the images were separated into three groups: 60 images and a separate set of 20 images were used for classifier training, while 20 images were used for evaluation.

As development environment, PyCharm from JetBrains was used for the programming language Python 3. The calculations were carried out on a MacBook Air OS X Yosemite Version 10.10.5 with a 1.4 GHz Intel Core i5.

4.2 Preprocessing Methods

All steps of the pattern recognition pipeline (see Figure 4.1) are necessary for the segmentation of the histology slices. In the preprocessing step, the images were prepared in a way that information about the PE particles and the CD3-positive cells is extracted (see Figure 4.2). In the following

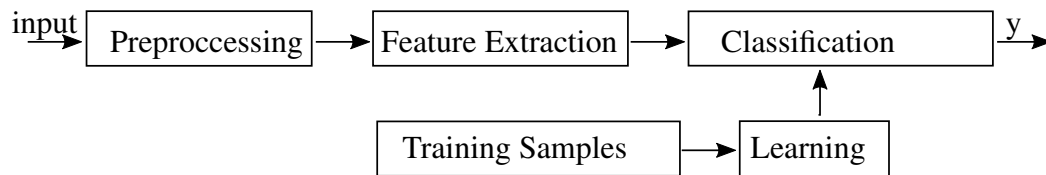


Figure 4.1: Pattern recognition pipeline for simple patterns [Pau98]

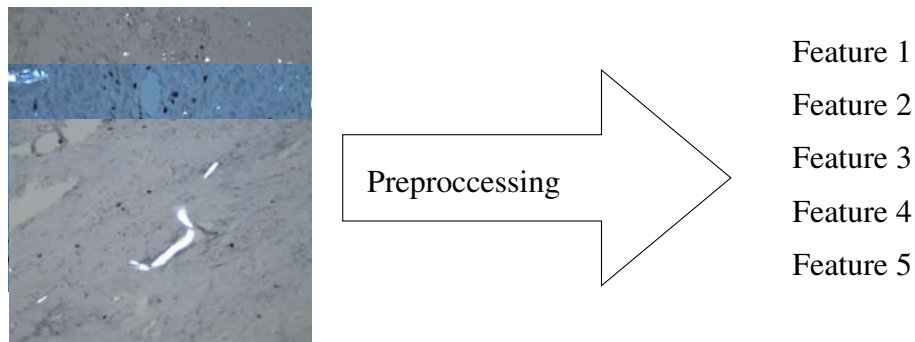


Figure 4.2: Preprocessing

subsections the preprocessing methods for containing the features of the CD3-positive cells and PE particles are presented.

4.2.1 Normalization

Color variation in tissue appearance caused by the staining of the histological images is a major problem for the computerized segmentation. It is not possible to choose a single threshold, which yields good results for the segmentation of all occurring stains within but also in between the images. Reasons for color variations are manifold. They are mostly caused by inconsistencies in the preparation, for example due to variations in cut thickness or the concentrations of the chemicals used for staining [Kha14]. In Figure 4.3 four examples from the 100 received images are displayed. Although they have been colored and prepared equally, the images contain a high variation in color and brightness. To solve this problem, it is necessary to standardize the histological slides. In literature, different approaches for the standard H&E staining of medical

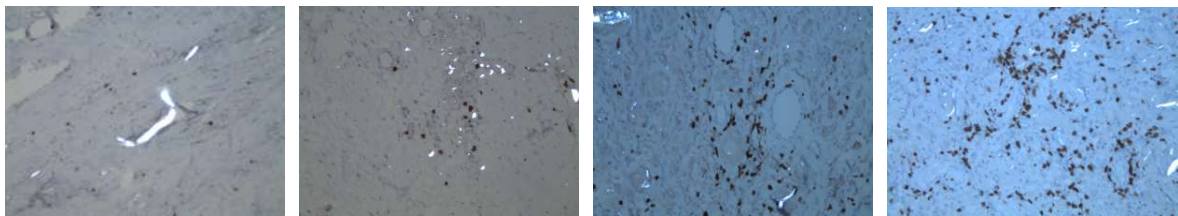


Figure 4.3: Different histopathological images with a high variation in color and brightness

histological images can be found. Thereby hematoxylin results in a blue-purple hue and stains colored by eosin are visible in a bright pink color. But the images received for this thesis were not colored with the usual H&E staining, because eosin would lead to a worsening of the recognition of the CD3-positive cells. Nevertheless, two normalization algorithms, Macenko [Mac09] and Reinhard [Rei01] normalization, which were successful used for H&E stained images, were evaluated and yielded good results. They will be described in detail in the following.

Macenko Normalization

This section handles the normalization method proposed by Macenko et al., which was used in [Mac09] on H&E slides of melanomas and nevi. In the main normalization step, it maps the calculated stain concentration matrix of the source image to the calculated stain concentration matrix of a target image using a linear per-channel normalization method. In the stain normalization toolbox of Warwick [ToW15], it is possible to choose different target images. In the scope of this thesis, the same target images was set the whole set of data, as it was desirable to obtain data with the same color and intensity.

In the following, each step of the Macenko normalization will be discussed. In case of a selectable target images steps 1 to 5 must be also done for the target image.

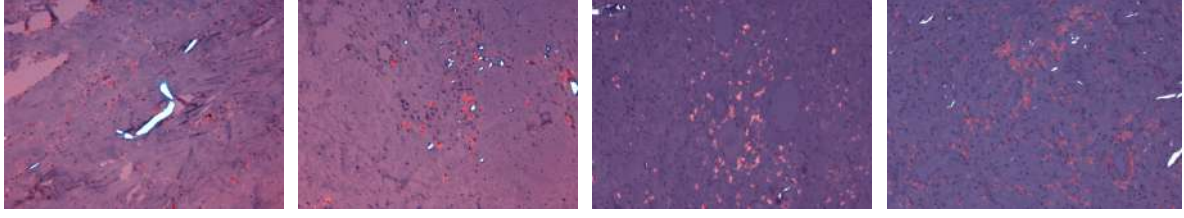


Figure 4.4: Macenko normalized histopathological images with a high color and intensity variation

- Step 1:

The RGB image is converted to optical density space (OD):

$$\mathbf{I}_{OD} = -\log_{10}(\mathbf{I}_{RGB}), \quad (4.1)$$

where \mathbf{I}_{RGB} stands for the RGB color vector containing the three channels normalized to $[0, 1]$ and \mathbf{I}_{OD} for the resulting RGB image in OD space. The transformation to the OD space makes a linear separation of colored stains (normally colored by the hematoxylin and the eosin) possible. As a result, a linear combination of stains leads to a linear combination of OD intensity values.

- Step 2:

The intensity values below a threshold β were set to 0, as they are assumed to have not been colored by eosin or hematoxylin and therefore do not contain a stain. According to Macenko et al. $\beta = 0.15$ yields the most robust results.

- Step 3:

The stain separation matrix with columns corresponding to the stain vectors is calculated. The two largest eigenvalues of \mathbf{I}_{OD} are determined using singular valued decomposition (SVD):

$$\mathbf{OD} = \mathbf{V}\mathbf{S} \quad (4.2)$$

$$\mathbf{S} = \mathbf{V}^{-1}\mathbf{OD}, \quad (4.3)$$

Where \mathbf{V} and \mathbf{S} are the matrices of the stain vectors. Corresponding to the eigenvalues, a plane is spanned in these directions. Now, the data is projected onto the plane and, after that, normalized to unit length. Then the angle of each point to the first SVD direction is then calculated. The resulting output are the optimal stain vectors in OD space.

- Step 4:

The stain concentrations for each channel in OD space are separated from the above calculated optimal stain vectors with the help of a color deconvolution (see more in Chapter 4.2.2 page 19)

- Step 5:

The robust extremes of the stain concentration for each channel are calculated with the use of the 99th percentile and the $(100 - \alpha)$ th percentile of the vectorized stain concentration. Empirically $\alpha = 1$ leads to robust extremes, but because of noise a robust result can be only reached by $\alpha = 0.99$.

- Step 6:

The main linear per-channel normalization based on the above calculated pseudo-maximum corresponding to α takes place. The source image values are mapped to match the target image values.

- Step 7:

In the last step, the RGB image is reconstructed. The output is the normalized RGB image [Mac09] [Kha14]. In Figure 4.5, the chosen target image, which is part of the color stain toolbox

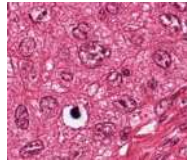


Figure 4.5: Chosen target image for Macenko Normalization [ToW15]

of Warwick, is shown. It contains the typical stain color concentrations for a H&E colored image. As already mentioned above, in this thesis, only this target image was used for all images. In Figure 4.4, the four different images from Figure 4.3 are normalized by Macenko et al. [Mac09]. There are less variations in color and brightness within the images. The CD3-positive cells are visible as red dots, the PE particles are clearly visible as bright regions and the background is colored more or less purple. Nevertheless a small variation in color and intensity persists. This could be due to excessive noise (e.g. saturated pixels). Also the target image was provided by the toolbox and not chosen for the application specifically, as no target images were available [Mac09] [Kha14].

Reinhard Normalization

In 2001 Reinhard et al. [Rei01] proposed a linear color correction method, where the standard deviation and mean of the three channels of the original image are matched to the corresponding channels of the target image. It is a simple and fast normalization algorithm, which was originally used for landscape images. Before the main matching is done, both images are converted from RGB to LAB colorspace [Rei01]. It has been already implied to digital histology images colored with the typical H&E staining [Mag09]. In the toolbox of Warwick, it is possible to choose different target images for the mapping. To minimize the computational effort, the means and standard deviations of the used target image are only calculated once and then added to the algorithm as fixed parameters. For calculating the parameters of the target image, step 1 and 2 had to be carried out for the target image. In the following, each step of the Reinhard normalization will be discussed:

- Step 1:

The RGB color space of the image is converted to Lab colorspace.

- Step 2:

The means and standard deviations of each channel of the image are calculated.

- Step 3:

The main normalization takes place. For each channel, the original color values are subtracted from the means of the source image. After this, the calculated value is divided by the standard deviation of the source image and multiplied with the standard deviation of the target image. At last, the mean of the target image is added. In the equations (4.4), (4.5) and (4.6), the normalization steps for the three channels of the Lab space are represented.

$$\mathbf{L}_{norm} = \frac{\mathbf{L}_{source} - \mu_{L_{source}}}{\sigma_{L_{source}}^2} \sigma_{L_{target}}^2 + \mu_{L_{target}} \quad (4.4)$$

$$\mathbf{A}_{norm} = \frac{\mathbf{A}_{source} - \mu_{A_{source}}}{\sigma_{A_{source}}^2} \sigma_{A_{target}}^2 + \mu_{A_{target}} \quad (4.5)$$

$$\mathbf{B}_{norm} = \frac{\mathbf{B}_{source} - \mu_{B_{source}}}{\sigma_{B_{source}}^2} \sigma_{B_{target}}^2 + \mu_{B_{target}} \quad (4.6)$$

L_{norm} , A_{norm} and B_{norm} are the normalized channels of the source image, L_{source} , A_{source} and B_{source} are the channels of the original image in Lab color space, μ_L , μ_A and μ_B are the means of the channels and σ_L^2 , σ_A^2 and σ_B^2 are the standard deviations for the channels.

- Step 4:

The normalized image is converted back from Lab colorspace to RGB colorspace. In Figure 4.6, the four images from Figure 4.3 are normalized with the help of this normalization method. The differences in color and brightness have disappeared. The CD3-positive cells are clearly visible as brown dots. The PE particles are colored bright, but also some areas of the background have a bright color. Especially in the third image from right side, the background has big bright areas. In

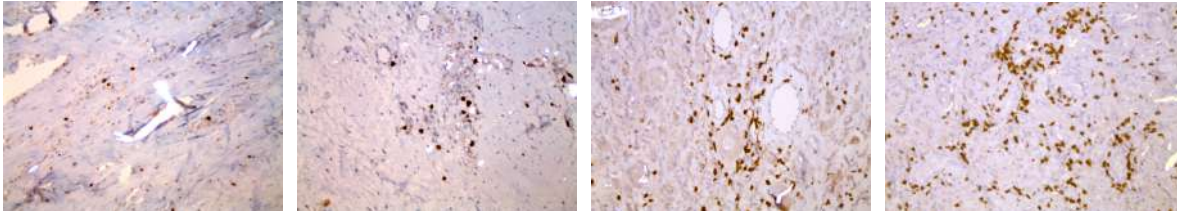


Figure 4.6: Reinhard normalized histopathological images

Figure 4.7, the used target image for the Reinhard normalization is shown. This image was used in [Mag09] for images of colorectal carcinoma stained with antibodies against CD34 [Kha14] [Mag09] [Rei01].

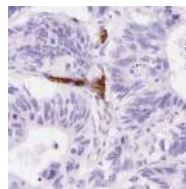


Figure 4.7: Chosen target image for Reinhard normalization [Mag09]

4.2.2 Color Deconvolution

Color deconvolution (CD) can be used to separate a RGB image into three channels. Thereby the channels represent the actual color of the stains [Kha14]. In the following, the two main steps of the CD will be discussed.

- Step 1:

First the RGB colorspace Ψ is transformed to a new colorspace $\hat{\Psi}$ corresponding to the Lambert-Beers law [Kha14]:

$$\Psi = \exp(-S\Psi) \quad (4.7)$$

$$\hat{\Psi} = S^{-1}(-\log \Psi) \quad (4.8)$$

with S defining the stain vectors [Kha14]

$$S = \begin{pmatrix} \bar{s}_{r1} & \bar{s}_{g1} & \bar{s}_{b1} \\ \bar{s}_{r2} & \bar{s}_{g2} & \bar{s}_{b2} \\ \bar{s}_{r3} & \bar{s}_{g3} & \bar{s}_{b3} \end{pmatrix}, \quad (4.9)$$

where $\bar{s}_{ri}, \bar{s}_{gi}, \bar{s}_{bi}$ stands for the normalized red, green and blue i -th normalized channel. After that, with the help of the stain matrix M , the concentrations of each stains are determined by dividing the reshaped image y_{OD} in OD color space by the stain matrix:

$$C = \frac{y_{OD}}{M} \quad (4.10)$$

- Step 2:

In the second step, the pseudo-color stain images for each channel are determined. Therefore again the stain matrix is used together with the in step 1 calculated deconvolved image for calculating the color for each stain.

$$CH_1 = I_0 \cdot \exp(C_1 \cdot (-M)) \quad (4.11)$$

$$CH_2 = I_0 \cdot \exp(C_2 \cdot (-M)) \quad (4.12)$$

$$CH_3 = I_0 \cdot \exp(C_3 \cdot (-M)) \quad (4.13)$$

CH_1, CH_2 and CH_3 represent the three deconvolved channels and I_0 is a variable with a fix value of $I_0 = 255$. In the general case of H&E colored stains, the first channel CH_1 stands for the haematoxylin stains, the second channel CH_2 for the eosin colored stains and the third channel CH_3 for the background. C_1, C_2 and C_3 stand for the three channels of the deconvolved image C in step 1. In the case of H&E staining, the background channel has to be white if the CD

was successful. For finding both PE particles and CD3-positive cells, CD was used. In case of extracting PE particles, the stain matrix:

$$M = \begin{pmatrix} 0.644211 & 0.716556 & 0.266844 \\ 0.092789 & 0.954111 & 0.283111 \end{pmatrix} \quad (4.14)$$

was used, for finding CD3-positive cells the stain matrix:

$$M = \begin{pmatrix} 0.3169 & 0.5971 & 0.7213 \\ 0.6361 & 0.7035 & 0.3509 \end{pmatrix} \quad (4.15)$$

was used.

Both these stain matrices were extracted out of the target images. In Figure 4.8 the CD into the

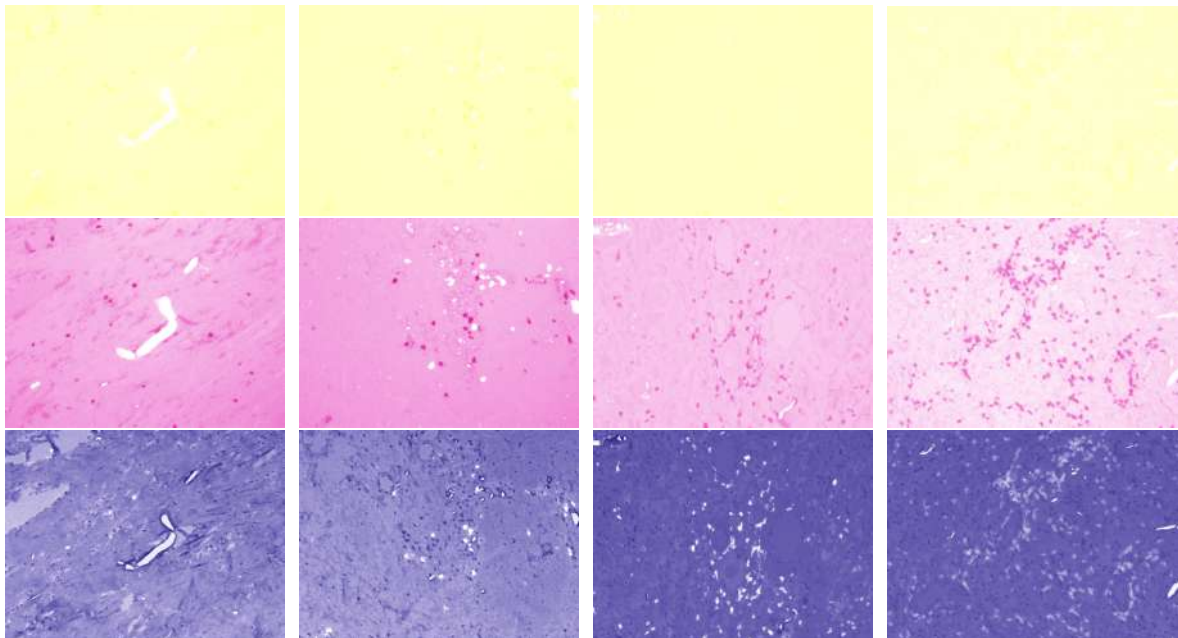


Figure 4.8: Color deconvolution of Macenko normalized images

three channels is shown for the Macenko normalized examples from Figure 4.4. Thereby channel 1 of the deconvolved images is presented in the top, the second deconvolved channel in the middle and the third deconvolved channel on the bottom. In this special case of stain coloring, a part of the CD3-positive immune response is visible in all three channels. In case of the first channel the CD3-positive cells are dark yellow to yellow on yellow background. In this channel, it is not possible to detect CD3-cells for all images. In case of the second channel the CD3-positive cells are dark pink on a pink background, in many cases it seems to be possible to detect most of the CD3-positive cells, but nevertheless Reinhard et al. allows a much better detection of

the CD3-positive cells (see Figure 4.10). In the third channel, the CD3-positive cells are bright dots, but also the PE is visible as white regions. In this channel, it is not possible to detect the CD3-positive cells.

For the detection of the PE particles, Macenko normalization followed by a CD yields good results. Therefore, a good segmentation of PE particles can be obtained by catching the second channel. Thereby nearly all PE particles, especially the MPE particles, are visible as bright areas on a pink background. When the visibility of the particles is compared with the images without CD (Figure 4.9), it is clear that particles can be detected better. Nevertheless, in some cases, the images are very noisy. In this cases, some parts of the background are colored white in addition to the PE particles. It is then advisable to take directly the Macenko normalized images without CD for thresholding.

For example in Figure 4.8 in the middle, the rightmost image is noisy, the PE particles become blurred with the background and as a consequence, the mean value is very high. In Figure 4.9 the

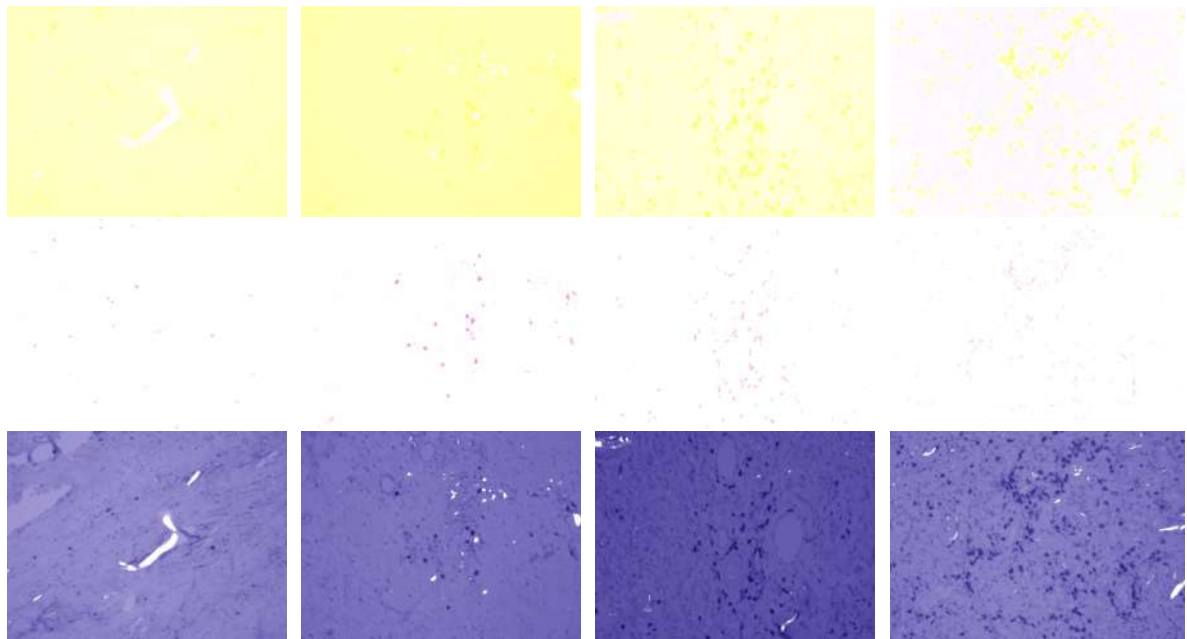


Figure 4.9: Color Deconvolution of the original images

CD of the original images without normalization is displayed. The first channel, which normally represents the background varies a lot, in all four images it contains information about the PE particles (white areas) and the CD3-positive immune response (dark yellow dots). In the right case, it even represents only the CD3-positive cells as strong yellow colored dots, which should be only the case in the second channel. The second channel presents the information about the CD3-positive cells as pink dots, only in the right case, the dots are somewhat weaker in the

color, but nevertheless visible. In the third channel most of the PE particles are visible as white areas. Compared with the visibility of PE particles in the second channel of the normalized color deconvolved image it has worse results. In Figure 4.10, the CD into three channels of the Reinhard

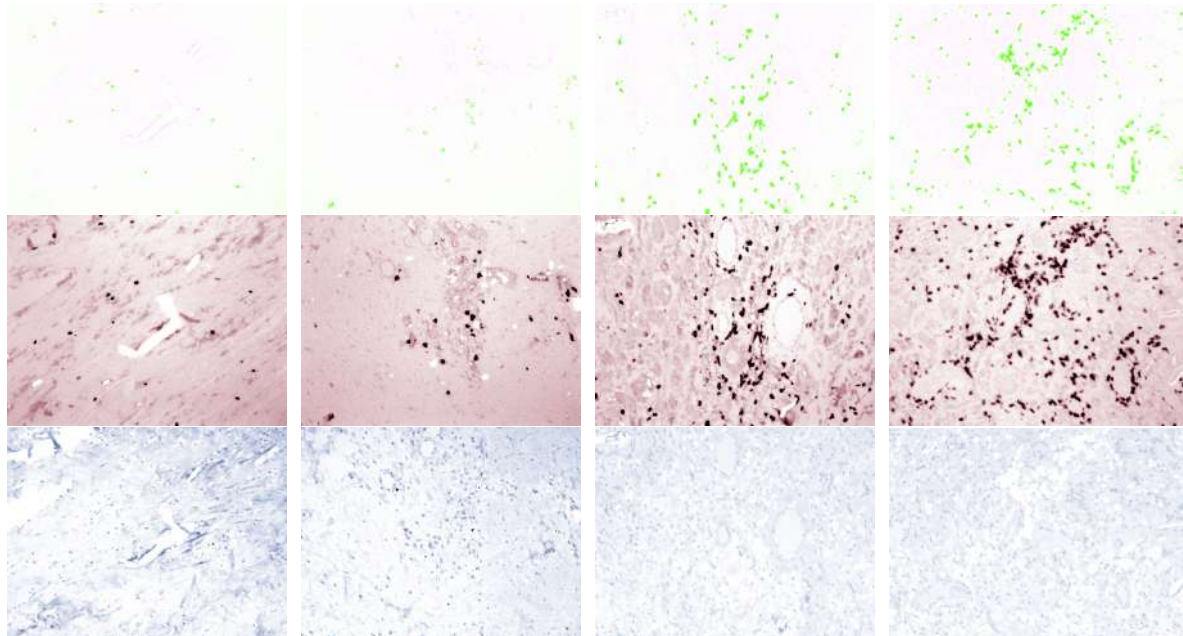


Figure 4.10: Color Deconvolution of Reinhard normalized images [Kha14]

et al. normalized images is shown. The first and the third channel do not need to be considered further, because both channels neither provide meaningful information about the CD3-positive cells nor about PE particles. However, in the second channel, the CD3-positive cells stand out clearly as dark brown dots from the bright background. PE particles are also presented in the second channel. Because of the confusion danger with salt noise and upcoming white regions of the CD, the detection of the PE particles with the Reinhard normalization yields a number of MacroPE/SMPE and MPE that is too high.

All in all, CD of the Macenko normalized images is quite important for finding the PE particles, which sometimes disappeared in the CD without normalization [Kha14].

4.2.3 Thresholding

After the image normalization and CD, it is possible to threshold the images with a simple binary threshold to contain the PE particles and CD3-positive cells as white regions on a black background.

Therefore, for finding the PE particles, the second channel of the color deconvolved grayscale

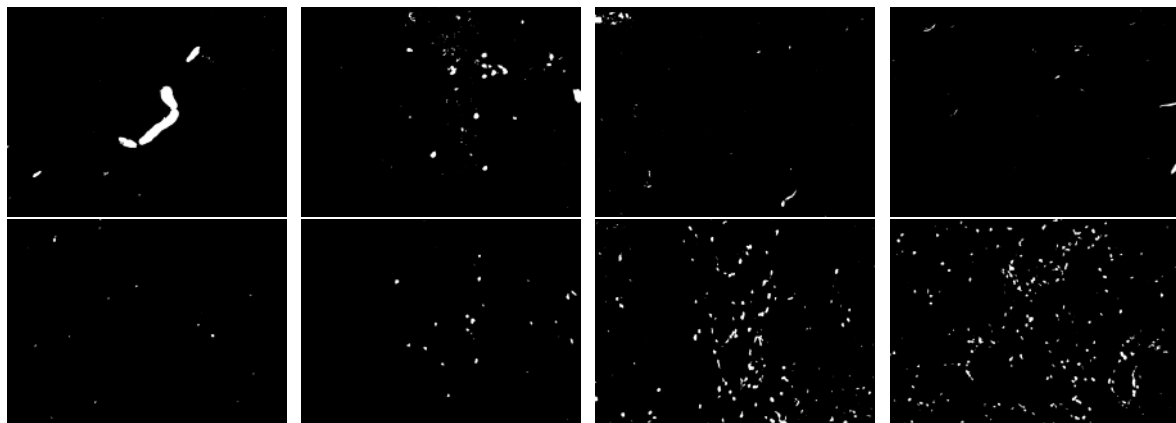


Figure 4.11: Top: Binary thresholding of the second channel of the Macenko normalized color deconvolved images for finding the PE particles; Botton: Binary thresholding of the second channel of the Reinhard normalized color deconvolved images for finding the CD3-positive cells

Macenko normalized image is thresholded with a fix threshold of 242.

As a result, the PE particles were colored white. Unfortunately, in some cases, the Macenko normalization followed by a CD failed. In this cases, after thresholding in addition to the PE particles, big parts of the background were colored white in the binary image. To solve this problem, in cases of a high mean value and a high number of detected PE, the gray-scaled Macenko normalized images are instead used for binary thresholding with a fix threshold of 230. The threshold is chosen smaller, because in the case of normalization without color deconvolution, the PE particles still vary in intensity values.

The CD3-positive immune/inflammatory response can also be detected by a fixed binary threshold of 100 on the second channel of the color deconvolved Reinhard normalized image followed by taking the inverse of the binary image. To determine the appearing noise and small dots, which cannot be CD3-positive cells due to their size, a median filter was used. In Figure 4.11, the results of the binary thresholding for the PE particles (top) and for the CD3-positive immune/inflammatory response are shown. The PE particles as well as the CD3-positive cells are now visible as white regions on a black background.

4.2.4 Morphological operations

Because of small black holes within and cracks inbetween some larger PE particles, it is necessary to use morphological operations. In 1964, mathematical morphology was developed by Georges Matheron and Jean Serra [Ron06]. As basic idea structure elements, i.e. small binary images with a simple predefined shape, are used to probe a binary image. Therefore, different shaped

structure elements are possible depending on how the shape of the white areas of the binary image should be changed. Before the morphological operation is applied on the image the basic and most important operations, Erosion, Opening, Dilation and Closing, will be explained briefly.

The morphological erosion of an image $A \in \mathbb{Z}^2$ by the structure element B is defined as [Gho14]:

$$A \ominus B = \{z \mid (B)_z \subseteq A\} \quad (4.16)$$

The morphological erosion minimizes the relation to every pixel in its neighborhood of every pixel. In contrast, the morphological dilation is defined as [Gho14]:

$$A \oplus B = \{z \mid (\hat{B})_z \cap A \neq \emptyset\} \quad (4.17)$$

where \hat{B} denotes the symmetric of B . A dilation minimizes the value of each pixel in relation to its neighboring pixels.

As a consequence, dilation enlarges bright regions and shrinks dark regions.

The morphological opening is a combination of a erosion followed by a dilation. Therefore an opening is defined as [Dou92]:

$$A \circ B = (A \ominus B) \oplus B^T. \quad (4.18)$$

It removes small bright spots and connects small dark cracks.

The morphological closing is defined as [Dou92]:

$$A \bullet B = (A \oplus B) \ominus B^T. \quad (4.19)$$

It is a dilation followed by an erosion. Closing makes it possible to remove small dark dots, which are smaller than the white particle, as well as to connect small bright cracks.

For removing the salt noise and the small holes, as well as continue SMPE/MacroPE particles, which lie very close to each other, a morphological closing, followed by a small median filter, was used. With the help of a cross-shaped kernel as structure element of a fixed size of (27,27), it was possible to close small black occurring holes and to continue PE particles, which are very close to each other. As the name already said, the form of the cross-shaped kernel corresponds to the shape of a cross (see Figure 4.12). In Figure 4.13, in the top a morphological closing, followed by a median filter is used to connect PE particles from the example images in the top from Figure 4.11. The particles are very close to each other and noise is present. After morphological closing,

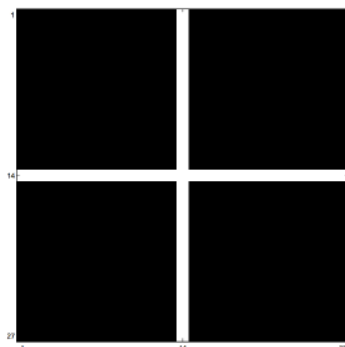


Figure 4.12: Structure element

the noise is reduced and the particles are separated. A median filter with a size of two yielded good results. In case of finding the CD3-positive cells (see images in the bottom from Figure 4.11) morphological operations were not necessary. To reduce the white noise a median filter with a size of ten achieved good results [Tea] [Gho14] [Dou92].

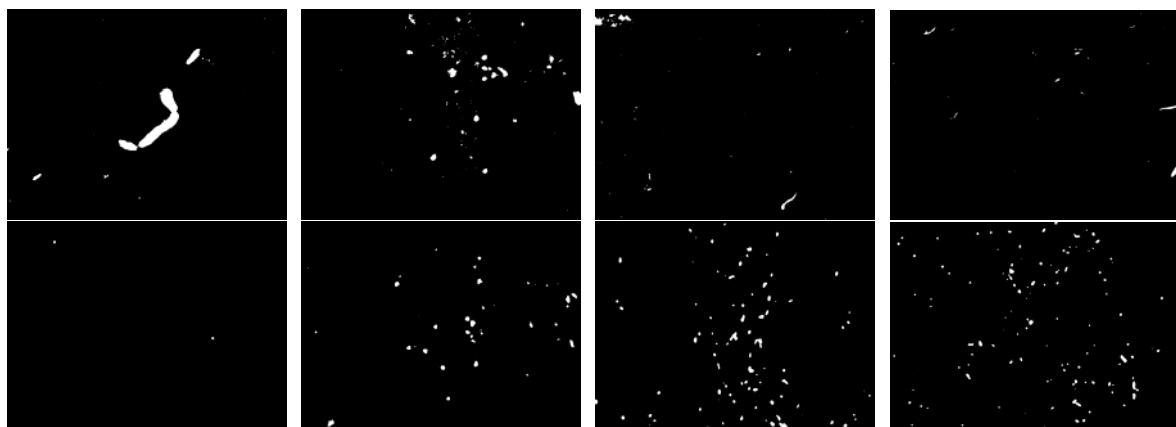


Figure 4.13: Top: Closing followed by a small median filter for finding PE particles; Bottom: Median filter for reducing white noise for finding CD3-positive cells

4.2.5 Blob detection

Blob detection algorithms are used for finding regions of interest, called blobs, which are similar in brightness, shape or color in an image. The most common methods for finding blobs are based on convolution [Tea17b] [Lin98] [Low04].

For finding the features of PE particles, a simple contour finding method was used. For finding the features of the CD3-positive immune/inflammatory response, a circular blob detection method,

the difference of Gaussian (DoG), has achieved good results. DoG is an efficient implementation of the Laplacian of Gaussian (LoG) approach, where two Gaussian blurred images $L(\mathbf{x}, \mathbf{y}, k\sigma)$ and $L(\mathbf{x}, \mathbf{y}, \sigma)$ are subtracted from each other [Low04]:

$$DoG(\mathbf{x}, \mathbf{y}, \sigma) = L(\mathbf{x}, \mathbf{y}, k\sigma) - L(\mathbf{x}, \mathbf{y}, \sigma) \quad (4.20)$$

$DoG(\mathbf{x}, \mathbf{y}, \sigma)$ is the difference of Gaussian, $L(\mathbf{x}, \mathbf{y}, \sigma)$ is the image $I(\mathbf{x}, \mathbf{y})$ convolved with a Gaussian $G(\mathbf{x}, \mathbf{y}, \sigma)$ [Low04]

$$L(\mathbf{x}, \mathbf{y}, \sigma) = G(\mathbf{x}, \mathbf{y}, \sigma) * I(\mathbf{x}, \mathbf{y}) \quad (4.21)$$

and $L(\mathbf{x}, \mathbf{y}, k\sigma)$ the image $I(\mathbf{x}, \mathbf{y})$ convolved with the Gaussian $G(\mathbf{x}, \mathbf{y}, k\sigma)$ [Low04]

$$L(\mathbf{x}, \mathbf{y}, k\sigma) = G(\mathbf{x}, \mathbf{y}, k\sigma) * I(\mathbf{x}, \mathbf{y}), \quad (4.22)$$

where $*$ denotes two-dimensional convolution. This is done with increasing standard deviations, the corresponding differences are stacked up in a cube. In the case of implementation blobs, are assumed to be white areas on a black background. As output, the number of blobs and the corresponding radii and coordinates of the midpoints of the blobs in the image are returned [Tea17b] [Lin98] [Low04]. For finding the contours, the areas, the coordinates of the center of mass and the numbers of the PE particles of the binary image, a simple contour finding method is used. Thereby the points, which corresponds to the contour are defined as a curve that fits all continues points of the boundary of each blob. Again, in case of implementation, the blobs, which correspond to the PE particles, are assumed to be white on a black background [Vis17] [Tea17a]. In Figure 4.14, the blob detection for the PE particles and the CD3-positive cells for the four images are shown. In the top, the PE particles are contoured red in the bottom the CD3-positive cells are marked in yellow. Nearly all of the CD3-positive cells are detected and marked. From left to right 31, 136, 20 and 229 CD3-positive cells were counted. Just in the cases of overlapping CD3-positive cells sometimes two or more cells are counted as one. The PE particles, especially the MacroPE and SMPE particles, are also more or less detected well. From left to right a total of 134, 61, 33 and 31 PE particles were counted. For the rightmost image this count is surly to small, not all PE particles were detected. For this image, the CD failed and therefore, instead of the second channel of the deconvolved image the Macenko normalized image was thresholded, which results in a worse detected number of PE particles.

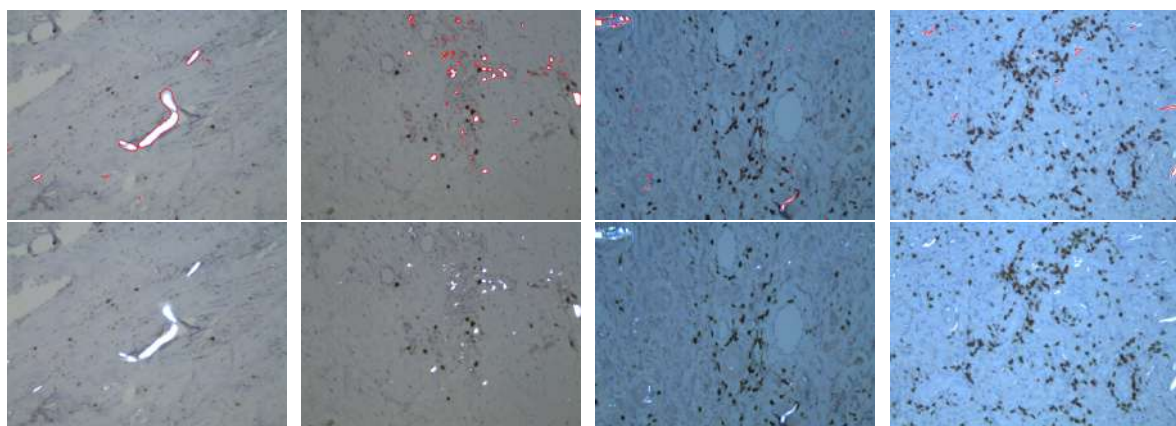


Figure 4.14: Top: Blob detection for finding PE particles; Bottom: Circular blob detection of the CD3-positive cells

4.2.6 Preprocessing Pipeline

For a better understanding, the most important steps of the image preprocessing of the histopathological slides are shown in Figure 4.15. For finding the CD3-positive cells it is necessary to

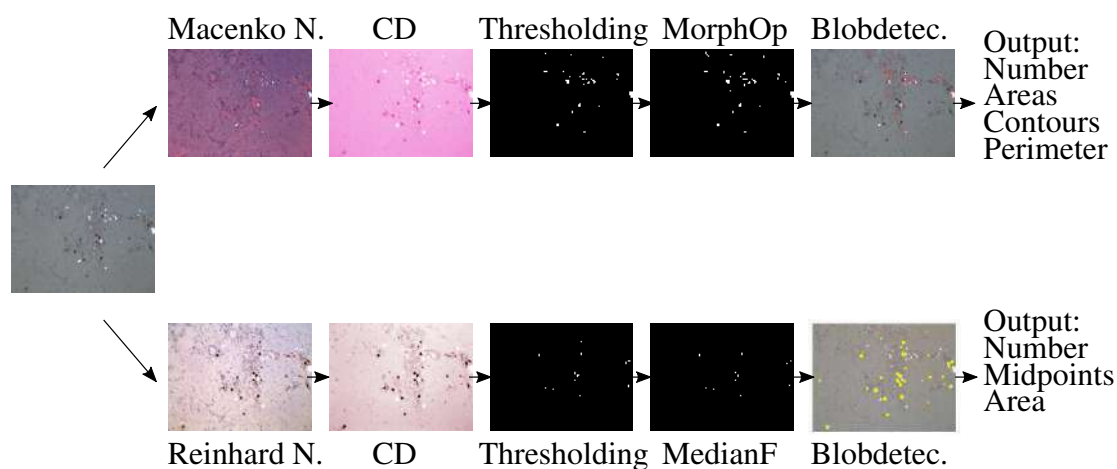


Figure 4.15: Preprocessing Pipeline

normalize the images and to deconvolve them into three channels. After that the gray-scaled second channel of the deconvolved image is used for thresholding. After the binary image is inverted and a circular blob detection method is applied the information about location, total area and number of CD3-positive cells per image is available.

To contain the features of PE particles, similar steps must be implemented. First, the images have

to be normalized. After that the images are color deconvolved. After that, the corresponding second gray-scaled channel is thresholded. With morphological operations, it is possible to reduce noise and to continue adjacent PE particles.

With a final simple blob detection the searched information, areas, perimeters, contours and the numbers of PE particles, could be obtained.

4.3 Classification Methods

After the preprocessing methods have been completed, it is necessary to extract suitable features (see section 5.1) as next step of the pattern recognition pipeline. The third step of the pattern recognition pipeline is the classification (see Figure 4.1). In frame of this thesis different supervised classifiers were used. The naive Bayes (NB) classifier, the support vector machine (SVM), the random forest (RF) and at least a variation of the nearest neighbor (NN) classifier will be presented in the following subsections.

4.3.1 Naive Bayes classifier

The NB classifier is an often used and simple classification algorithm with a mostly good performance. Similar to the Bayesian classifier it decides for the class according to the decision rule [Nö15]

$$y^* = \operatorname{argmax}_y p(y|\mathbf{x}) \quad (4.23)$$

but with the simplification assumption of the independence between the features, which implies [Nö15]

$$p(\mathbf{x}|y) = \prod_{i=1}^d p(\mathbf{x}_i|y) \quad (4.24)$$

and results in the decision rule of Naive Bayes [Nö15]:

$$y^* = \operatorname{argmax}_y p(y|\mathbf{x}) = \operatorname{argmax}_y p(y) \prod_{i=1}^d p(\mathbf{x}_i|y) \quad (4.25)$$

where y represents the class number, \mathbf{x} the feature vector, $p(y)$ the prior probability of class y , $p(\mathbf{x}|y)$ the joint probability function and $p(y|\mathbf{x})$ the class conditional density [Bis06] [Nö15].

4.3.2 Support vector machines

A support vector machine is a linear classifier for separating classes with the help of points to the line for each class. The decision boundary is defined as an affine function [Nö15]:

$$f(\mathbf{x}) = \boldsymbol{\alpha}^T \mathbf{x} + \alpha_0 \quad (4.26)$$

where \mathbf{x} is any point and the normal vector \mathbf{n} of the hyperplane is defined as [Nö15]:

$$\mathbf{n} = \frac{\boldsymbol{\alpha}}{\|\boldsymbol{\alpha}\|_2} \quad (4.27)$$

Two different forms of SVM are available, hard margin SVM with the optimization problem: maximize [Nö15]

$$\frac{1}{\|\boldsymbol{\alpha}\|_2} \quad (4.28)$$

subject to

$$\forall \mathbf{i} : y_i \cdot (\boldsymbol{\alpha}^T \mathbf{x}_i + \alpha_0) \geq 1 \quad (4.29)$$

and soft margin SVM with the convex optimization problem minimize [Nö15]

$$\frac{1}{2} \|\boldsymbol{\alpha}\|_2^2 + \mu \sum_i \xi_i \quad (4.30)$$

subject to

$$\forall \mathbf{i} : -(y_i \cdot (\boldsymbol{\alpha}^T \mathbf{x}_i + \alpha_0) - 1 + \xi_i) \leq 0 \quad (4.31)$$

$$\forall \mathbf{i} : -\xi_i \leq 0, \quad (4.32)$$

where y is the class number for all class labels \mathbf{i} , ξ is the slack variable and μ a weighting factor. In case of a hard margin problem, the classes are linearly separable. In case of the soft margin problem outliers exist and the classes are no longer linearly separable. In the following, because of occurring outliers, the soft margin SVM was used [Bis06] [Nö15].

4.3.3 Random Forest

Random forests is a fast supervised classification method, which consists of many weak learners. With the help of a decision tree, a general mapping for predicting the classes of a test set can be learned with the help of a labeled training set. Therefore, the parameters of the weak learners are

optimized at each split node j with [Cri13]:

$$\boldsymbol{\theta}_j = \operatorname{argmax}_{\boldsymbol{\theta}_j \in T_j} I(S_j, \boldsymbol{\theta}) \quad (4.33)$$

where S_j is the training set and $\boldsymbol{\theta}$ is the split parameter. The optimization function I for the classification can be described as [Cri13]:

$$I(S_j, \boldsymbol{\theta}) = H(S_j) - \sum_{i \in \{L, R\}} \frac{|S_j^i|}{|S_j|} H(S_j^i) \quad (4.34)$$

where $H(S)$ is the entropy [Cri13]:

$$H(S) = - \sum_{c \in C} p(c) \log p(c) \quad (4.35)$$

where $p(c)$ is the normalized histogram of labels corresponding to the points in S of the training-set for each node and i is the indexing of the two child nodes [Cri13].

4.3.4 Nearest Neighbor Classifier

In addition to the classification of the different PE particles and the strength of the MPE particles as well as the strength of the CD3-positive immune/inflammatory response a NN classifier is used for calculating the number of CD3-positive cells in a fix Euclidean distance of maximal $5 \mu m$ around the MacroPE/SMPE and the MPE particles, respectively.

Because of the different shapes of the PE particles, it is not suitable to use the midpoints or the center of mass of the MacroPE/SMPE particles, instead the contours of these particles were used. In case of the CD3-positive cells, because of the circular structure, the midpoints could be used (see also Figure 4.16). In Algorithm 1, the pseudocode is shown. As input the algorithm needs the contours of each MacroPE/SMPE particle per image (*contours*), the midpoints of all CD3-positive cells per image (X_{CD3}) and optionally the chosen distance (*distance*) between CD3-positive cells and MacroPE/SMPE particles. Normally the distance is initialized with $distance = 17.24$, which corresponds to a distance of $5 \mu m$ in pixels. As output, the NN algorithm returns the number of CD3-positive cells around the maximal Euclidean distance of $5 \mu m$ to all MacroPE/SMPE and to all MPE particles per image.

Therefore, first of all, the number and distance vectors, which will later contain all distances between one CD3-positive cell and the contour points of one MacroPE/SMPE for all CD3-positive

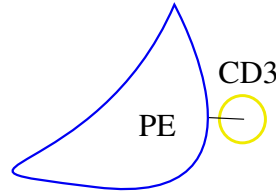


Figure 4.16: Distance Measure: blue object represents a PE particle, yellow object: represents one CD3-positive cell; the black line represents the minimal calculated distance between the contour of the PE particle and the midpoint of the CD3-positive cell

cells and for all MacroPE/SMPE particles, are initialized.

In the next step the distances are calculated with the help of the L2 norm and, after that, sorted according to the size, in which the smallest value stands in the first place.

A following 'if state' checks whether the smallest calculated distance is smaller than the predetermined distance of $5\mu m$. If it is true, the number of the CD3-positive cells, which are next to a MacroPE/SMPE particle is counted up by one [Bis06] [Nö15].

Algorithm 1 Nearest Neighbor Classifier

```

1: function  $num = \text{NEARESTNEIGBOR}(contour, X_{CD3}, distance = 17.24)$ 
2:    $num \leftarrow 0$  initialize number of adjacent cells with 0
3:    $dist \leftarrow \text{empty}(\text{len}(contour))$  initialize empty distance vector
4:   for  $i \leftarrow 0, \text{length}(X_{CD3})$  do
5:     for  $j \leftarrow 0, \text{length}(contour)$  do
6:        $dist[j] = \text{Norm}_{L2}(contour[j] - X_{CD3}[i])$  Calculate Euclidean Distance
7:     end for
8:   end for
9:   Sort  $dist$ 
10:  if  $dist[0] < distance$  then  $num = num + 1$ 
11:  end if
12: end function

```

4.4 Additional

For an easy handling, a simple graphical user interface (GUI) was designed and implemented with the above presented algorithms (see Figure 4.17). As input a histology image can be loaded via

the top right button 'Datei auswählen'. The two formats 'PNG' and 'JPEG' are supported. After a image was chosen, the program can be started by pressing the bottom right button 'Start'. The

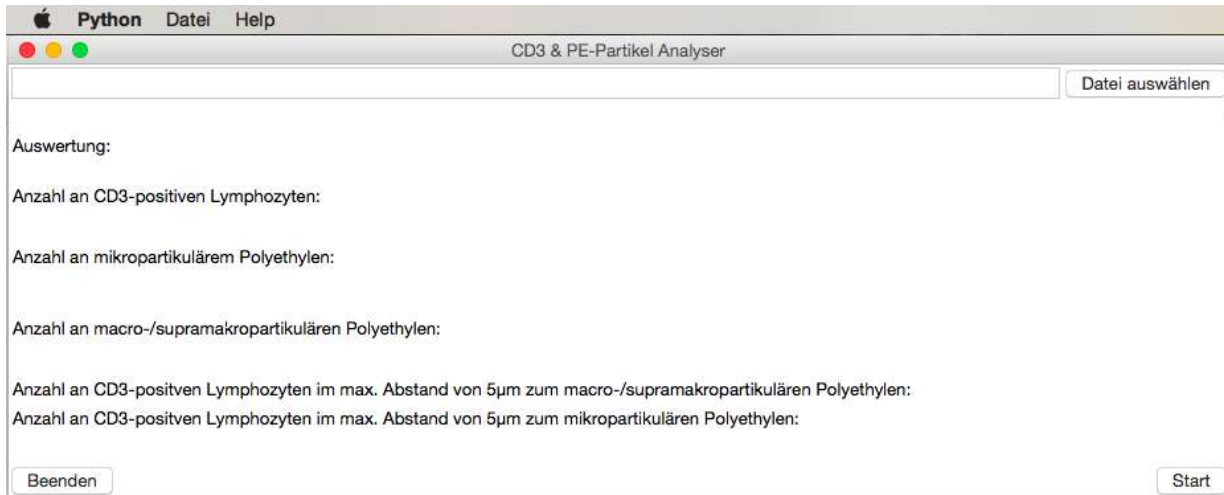


Figure 4.17: Graphical User Interface

program counts the number of MPE particles, MacroPE/SMPE particles and CD3-positive cells. Additionally the number of adjacent CD3-positive cells around the MacroPE/SMPE particles and MPE particles, respectively, are determined.

If the image contains no MacroPE/SMPE, or MPE particles, the distance measurement returns the remark that no MacroPE/SMPE, respectively MPE particles, are available. In addition to that, the chosen image appears with the colored marked particles and cells (see 4.18). The PE particles are colored blue and the CD3-positive cells are marked with yellow circles. For a better understanding for users without knowledge in this medical field, short explanations of characteristic features about the MacroPE/SMPE, MPE and CD3-positive cells are available. To obtain these information, the cursor of the mouse has to point to the text 'CD3-positive Lymphozyten', 'mikropartikuläres Polyethylen', or 'makro/supramakropartikuläres Polyethylen'.

Auswertung:

Anzahl an CD3-positiven Lymphozyten: 61

Anzahl an mikropartikulärem Polyethylen: 32

Anzahl an macro-/supramakropartikulären Polyethylen: 9

Anzahl an CD3-positiven Lymphozyten im max. Abstand von 5 μ m zum macro-/supramakropartikulären Polyethylen: 0

Anzahl an CD3-positiven Lymphozyten im max. Abstand von 5 μ m zum mikropartikulären Polyethylen: 3

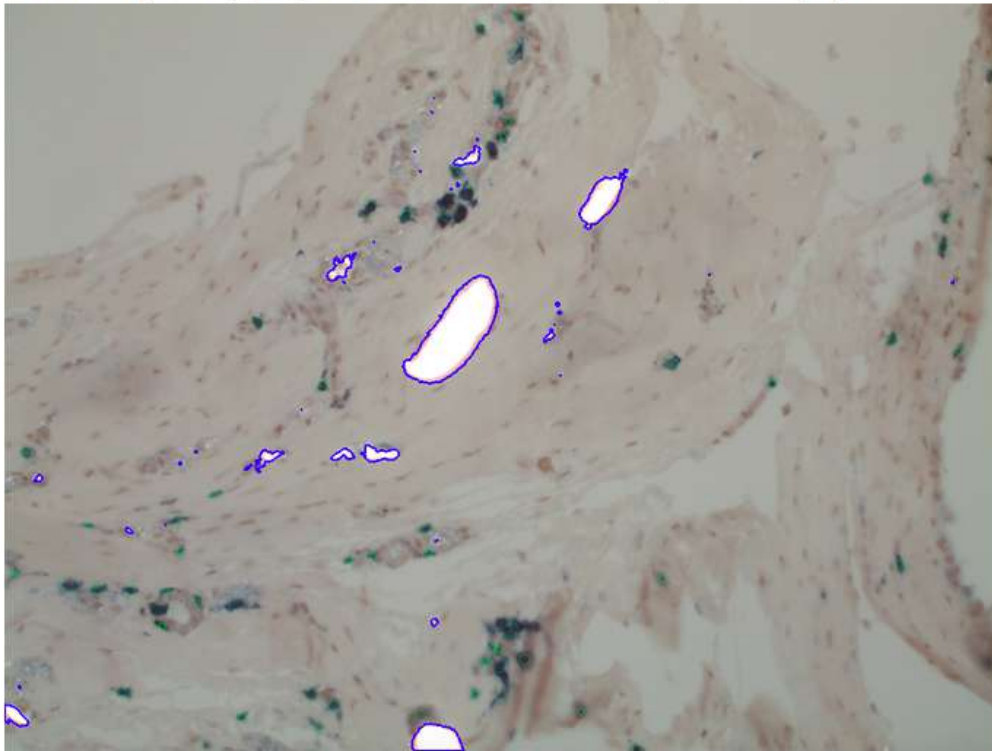


Figure 4.18: Graphical User Interface with the evaluation for a single image

Chapter 5

Results and Discussion

In the following chapter, the results that were achieved with the methods presented in 4.2 will be discussed. First, all of the suitable features obtained with the preprocessing steps will be shown. In the next step, the different classifiers introduced in chapter 2 will be used for classification of the particles and associated immune response: MPE particles were separated into low, moderate and high. CD3-positive cells were separated into low, moderate and high immune/inflammatory response and PE particles have to be divided into MPE and MacroPE/SMPE. After that, the obtained results about the relationships between MPE particles and CD3-positive immune/inflammatory response will be discussed.

5.1 Features

After the preprocessing of the 100 histopathological images, suitable features have been extracted. Therefore, the information gained from blob detection methods introduced in 4.2.5 were used.

5.1.1 Features of CD3-positive immune/inflammatory response

It was found out that for separating the CD3-positive immune/inflammatory response in the three classes, low, moderate and high, the absolute number and the total area share of these cells per image, are suitable (see Figure 5.1).

In Figure 5.2, the normalized numbers and areas of CD3-positive cells for the 60 training images, the 20 validation images and the 20 images for testing are shown from left to right. According to the predetermined ground truth data, the red dots correspond to a low, the blue ones for a moderate and the green dots for a high CD3-positive immune/inflammatory response. Therefore,

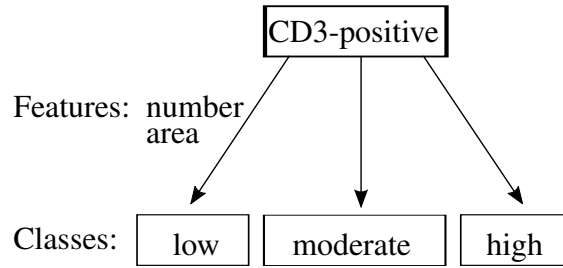


Figure 5.1: Features of CD3-positive immune/inflammatory response

every dot represents exactly one image. According to the expectations, the dots which are labeled

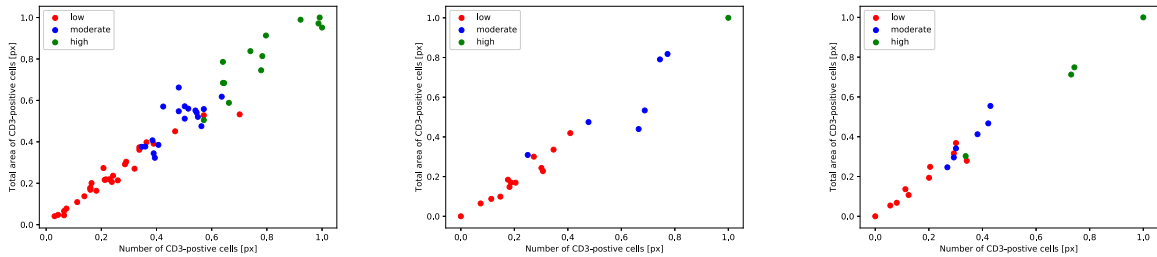


Figure 5.2: Left: CD3 features for training-set; middle: CD3 features for validation-set; right: CD3 features for all test data

with a low CD3-positive immune/inflammatory response lie mostly in the upper left corner of the graph. A small number of CD3-positive cells combined with a small total area share per image represents a low immune/inflammatory response. The dots labeled with a moderate response lie mostly in the middle of the graph. A moderate immune/inflammatory response is presented at an average number and total area share of the CD3-positive cells per image. The green dots are mostly separated in the upper right corner. Consequently, a high immune/inflammatory response is available for a high number and total area share of CD3-positive cells per image.

In the presented 100 images, the class with a high CD3-positive immune/inflammatory response is under-determined, as e.g. validation images only contain one element of this class. Overall, the classes are unequally distributed, class 'low' is most represented with 53 counts, followed by class 'moderate' with 30 counts. Class 'high' is only represented in 17 images. Furthermore, it is noticeable that in some cases, one class lies on the edge at another class or two classes are partially overlapping.

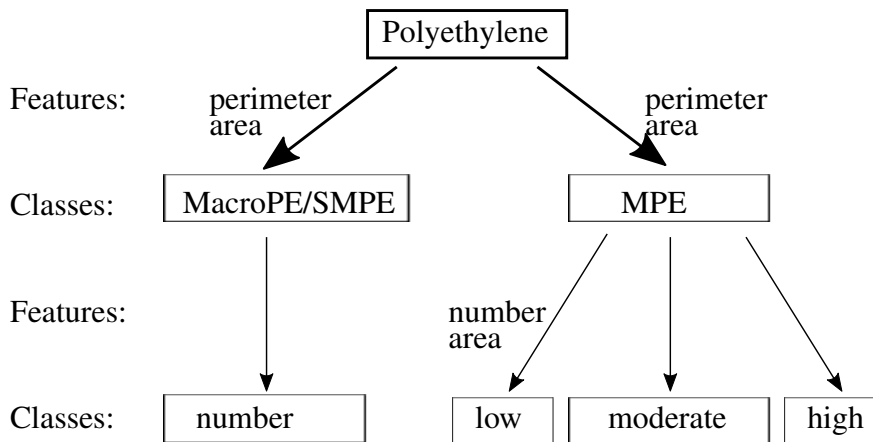


Figure 5.3: Features of PE particles

5.1.2 Features of PE particles

As features for separating the PE particles in MPE and MacroPE/SMPE, the perimeters and the total area occupied by PE particles per image were chosen as suitable features. For classifying the MPE particles into the three classes 'low', 'moderate' and 'high' it turned out that the number and the area of MPE particles per image are suitable. Because of the small amount of MacroPE/SMPE and the known number of them per image the pure numbers are used (see Figure 5.3). Because there exists no further information about whether a particle in the image is a MPE or a MacroPE/SMPE and only the information about the total number of MacroPE/SMPE and the classes about the MPE per image are available the following simplifying assumptions were made:

1. The 219 particles with the tallest perimeters of the training-set are MacroPE/SMPE particles
2. The 112 particles with the tallest perimeters of the validation-set are MacroPE/SMPE particles
3. The 39 particles with the tallest perimeters of the test-set are MacroPE/SMPE particles

These numbers corresponds to the known whole numbers of MacroPE/SMPE of the training-, test- and validation-images.

In Figure 5.4, the perimeters and areas of occupied PE particles in the data sets are shown for the training-, validation- and test-images (from left to right), split into MacroPE/SMPE (green dots) and MPE (red dots). In Figure 5.5, the PE particles in relation to their area and their perimeters are shown, but this time only for two single images. The image on the right side contains MPE (bottom left corner) as well as MacroPE/SMPE (middle). The image on the left side only contains MPE particles, which lie in the bottom left corner due their small sizes of perimeter and area.

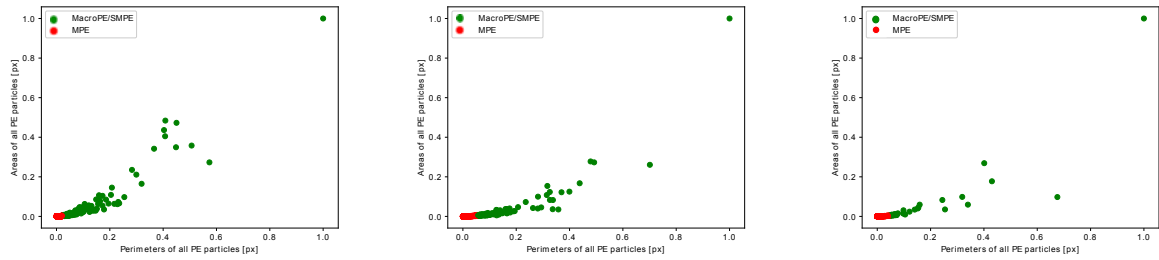


Figure 5.4: Left: PE features for trainingsset; middle: PE features for validationset; right: PE features for testset

After a separation of the PE particles into MacroPE/SMPE and MPE for all single images, the

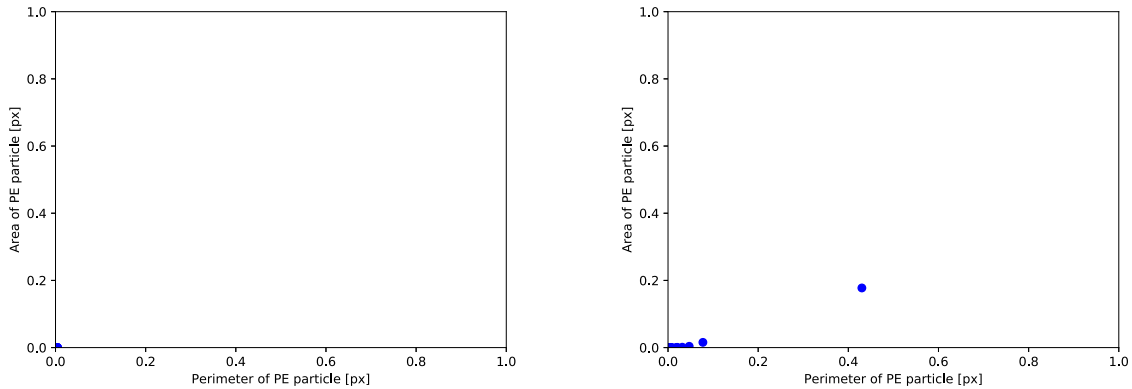


Figure 5.5: PE particle distribution for the features area and perimeter for two images

predicted number and total area of MPE per image are used as features for the classification of MPE into the three classes low, moderate and high (see Figure 5.6). The blue dots represent the class low MPE, the red ones the class moderate MPE and the green dots again the class high MPE. As it was to be expected from the analysis of the available data, the most cases the blue dots are located in the upper left corner, the red dots are located in the middle and the green dots are located in the upper right corner. In the cases of the validation- and test-set (see middle and right image in Figure 5.6), this classification is mostly successful, just some outliers are visible. In case of the training-images, presented in the left image in Figure 5.6), more outliers are present. Especially in the upper-left corner a mixture of all classes are occurring. For this phenomena two reasons are possible. Either, in some case, a certain number of MPE was not detected in the preprocessing steps or some MPE particles are not visible due to low image quality and compression effects introduced by lossy image codecs like 'JPEG'.

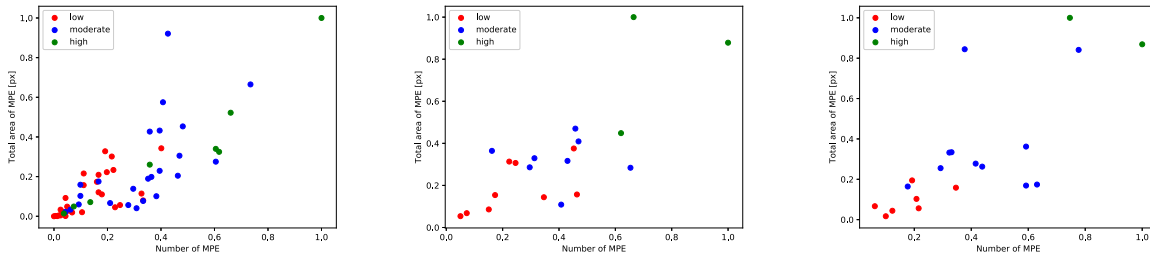


Figure 5.6: MPE features for training-, validation- and test-set (from left to right)

5.2 Classification

In this section, different supervised classification approaches are used on the features introduced in 5.1. They are used to separate the PE particles into MacroPE/SMPE and MPE, to separate MPE into low, moderate and high and to separate the CD3-positive cells into a low, moderate and high immune/inflammatory response (see Figure 5.3 and Figure 5.1).

5.2.1 Classification of CD3-positive immune/inflammatory response with Naive Bayes

Although the features of the CD3-positive immune/inflammatory response lie more or less on a diagonal and it can be thereby assumed that both features are correlated, a NB classifier as introduced in section 4.3.1 yielded reasonable results.

In Figure 5.7, the decision for the used NB classifier are shown for the data-sets. In the cases of

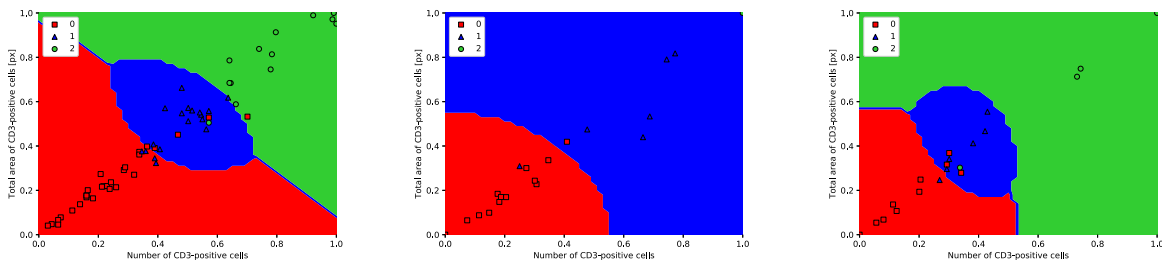


Figure 5.7: NB decision boundaries in the training, validation and test data sets (from left to right)

the training- and test-sets, most of the immune response are classified right. A point in the bottom left side of the graph will be associated to class 0, a point in the middle of the graph belongs to class 1 and therefore a point in the upper right side will be classified as class 2.

Because of the unequal distributions of labeled classes in case of the validation-set, class three is not be detected anymore, as the prior probability of this class was almost zero. Therefore, training with the validation-set only yielded good results for class 0 and 1.

But nevertheless, an accuracy of 70 % could be obtained with the validation data. With a training with the extracted features from the 60 images of the training-set an accuracy of 80 % can be reached.

In Table 5.1, the confusion matrix for the training of the NB classifier with the features of the 20 images of the validation-set is shown.

In most cases, the classes are classified right, but especially in cases of a ground truth class 2 the classification fails, as expected from the decision lines shown in Figure 5.7. Additionally, some points corresponding to class 1 are predicted as class 0. The reason of this failure is due to the increase a-priori probabilities caused by the unequal class distribution in the validation set. The class 0 occurs most frequently and therefore by training the probabilities for this class affiliations are chosen to high. In Table 5.2 the confusion matrix for the training of the NB classifier with the

truth: \ predicted:	Class 0	Class 1	Class 2
Class 0	10	0	0
Class 1	3	3	0
Class 2	1	2	1

Table 5.1: NB confusion matrix for training with the validation data set

extracted features of the 60 training-images are shown. Class 2 is now classified correctly in more cases. In comparison with the results of the confusion matrix shown in Table 5.1, the predicted

truth: \ predicted:	Class 0	Class 1	Class 2
Class 0	10	0	0
Class 1	3	3	0
Class 2	1	0	3

Table 5.2: NB confusion matrix for training with the training data set

classes are chosen similar, with the only difference of a better performance of the predicted class 2, due to a higher represented of class 2 in the training-set, this class is chosen correct in nearly all cases.

5.2.2 Classification of CD3-positive immune/inflammatory response with Support Vector Machines

The classification of the CD3-positive immune/inflammatory response with a SVM also yields acceptable results. With both the training and the validation data sets, an accuracy of 70 % could be reached. In Figure 5.8, again, the decision domains for the training-, validation- and test-set

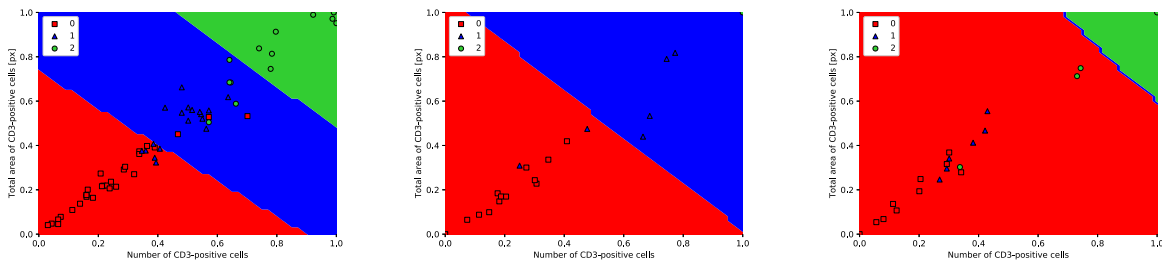


Figure 5.8: SVM decision boundaries in the training, validation and test data sets (from left to right)

are shown (from left to right). For the training-set it looks quite good, the three classes 0, 1 and 2 are equally separated. In comparison with the decisions made by the NB classifier for the training-set it looks equal good or even tend to be somewhat better. The decision for the validation-set looks similar, too. Class 0 and 1 are well separated, but the decision for class 2 is worse. However, the decision boundaries based on the test-set are much worse than for the NB classifier. In Table 5.3, the confusion matrix for the classifier training by the features of the validation-set is shown. It is identical to the confusion matrix for the NB classifier. Class 1 is chosen to often and class 2 to rarely. In the two confusion matrices shown in Table 5.3 and Table

truth:\npredicted:	Class 0	Class 1	Class 2
Class 0	10	0	0
Class 1	3	3	0
Class 2	1	2	1

Table 5.3: SVM confusion matrix for training with the validation data set

5.4, the predicted class numbers and ground truth numbers for the training and validation data sets are shown. As expected, in case of the validation-set, class 2 is not detected anymore. In case of the training-set, a similar distribution as with NB classifier can be reached. In Table 5.4, the confusion matrix is shown for the SVM classifier training with the features of the training data

truth: \ predicted:	Class 0	Class 1	Class 2
Class 0	10	0	0
Class 1	4	2	0
Class 2	1	1	2

Table 5.4: SVM confusion matrix for the training with the training data set

set. Class 2 is chosen well, nevertheless class 1 is chosen to often. In comparison with the NB confusion matrix it performance a little bit worse.

5.2.3 Classification of CD3-positive immune/inflammatory response with Random Forest

A classification of the CD3-positive cells with a RF classifier leads to good results with an accuracy of 80 %, for the training and 70 % for the validation data set. Nevertheless, with a look at the decision lines for the feature vectors of the training-set (shown in the left of Figure 5.9) it is visible that the decision domain for class 1 is separated. In case of the validation-set (shown in the middle of Figure 5.9) the class decision are suitable, despite the low a-priori probability for class 2. In

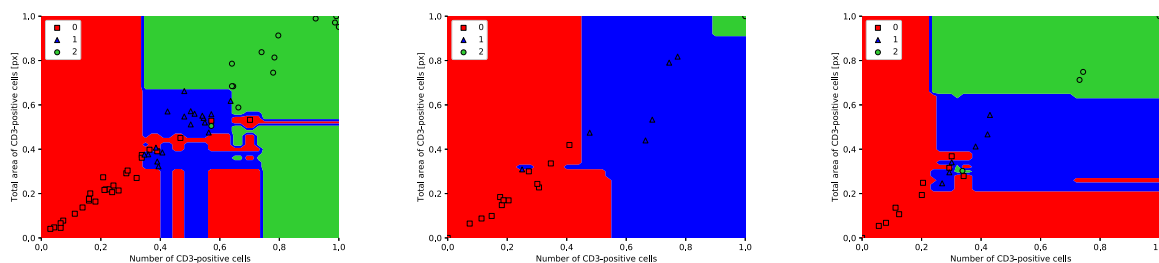


Figure 5.9: RF confusion matrix for the training with the validation data set

truth: \ predicted:	Class 0	Class 1	Class 2
Class 0	10	0	0
Class 1	3	3	0
Class 2	1	2	1

Table 5.5: RF confusion matrix for the training with the training data set

Table 5.9, the confusion matrix for a training with the available data of the validation-set is shown. The classes are chosen correctly, but, similar to the corresponding confusion matrices for NB and

SVM, class 2 is chosen too rarely and class 0 too often.

In Table 5.6, the confusion matrix for a training with the available data of the training-set is shown. The classes are mostly chosen correctly, only class 0 is chosen too often. All in all, it

truth:\predicted:	Class 0	Class 1	Class 2
Class 0	10	0	0
Class 1	3	3	0
Class 2	1	0	3

Table 5.6: RF confusion matrix for the training with the validation data set

can be said, that all classifiers perform similar, NB and RF reach a little bit better accuracy of 80% instead of 70 % by training with the features of the 60 training-images. But nevertheless a equal distribution of the classes would be desirable and leads to better results for all classifiers, especially for training with the features of the the validation-set.

5.2.4 Classification of PE particles with Naive Bayes

For separating the PE particles into the two classes MacroPE/SMPE and MPE, a NB classifier was used. Therefore the calculated areas and perimeters of all PE particles of the whole training-set, and the validation data set respectively, were used for fitting the classifier with the aimed information about the class correspondences taken of the assumptions made in 5.1.2. In Figure 5.10 the decisions chosen with the NB classifier for the training-, validation- and test-set are shown from left to right. After the training, the classifier is evaluated based on the predicted

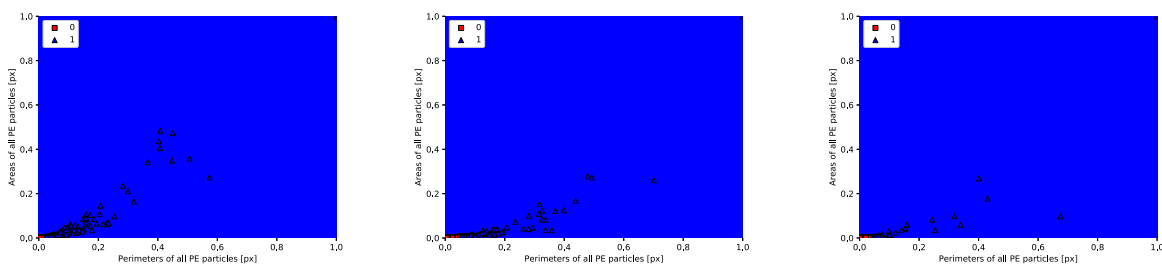


Figure 5.10: NB decision boundaries in the training, validation and test data sets (from left to right)

numbers of MacroPE/SMPE particles for each test image.

Based on the training data set it was possible to count the number of MacroPE/SMPE with an accuracy of 55 %. A standard deviation of 1 leads to an accuracy of even 90 %, increasing the standard deviation to 2 leads to an increased accuracy of 95 %. Based on the validation data set it was possible to count the number of MacroPE/SMPE with a similar, but little better, accuracy of 60 % were possible. Increasing the standard deviation to 1 leads to an accuracy of 85 %. A standard deviation of 2 leads to an accuracy of 95 %.

In Figure 5.11, the groundtruth number of MacroPE/SMPE versus the predicted number of MacroPE/SMPE are shown. On the left side, the classifier is trained with the training data set and on the right side with the validation data set.

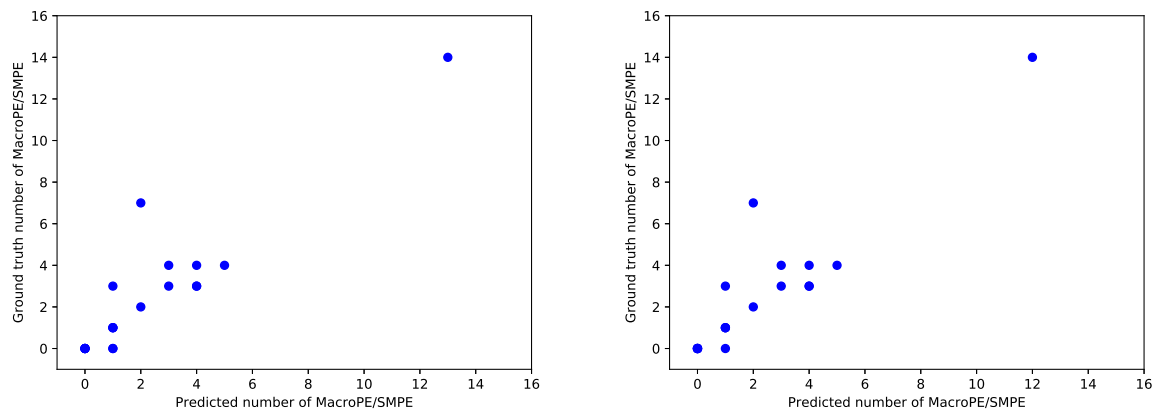


Figure 5.11: Groundtruth number of MacroPE/SMPE particles of Testdata versus predicted number of MacroPE/SMPE for training (left side) and validation data set (right side) with NB

5.2.5 Classification of MPE particles with Naive Bayes

For the classification of the MPE particles, the numbers of MPE particles and the total area of MPE per image were used. With both the training and validation data sets, the NB classifier achieved an accuracy of 80 %.

In Figure 5.12, the decision domains of the NB classifier are shown for the training-, validation- and test-set (from left to right). In all three cases, the decision domains corresponds mostly to the data. In Table 5.8 and Table 5.7, the confusion matrices for training with the training and validation data set are shown. In both cases, a similar distribution is given. All three classes were mostly predicted correctly, just in a few cases, class 1 was missclassified.

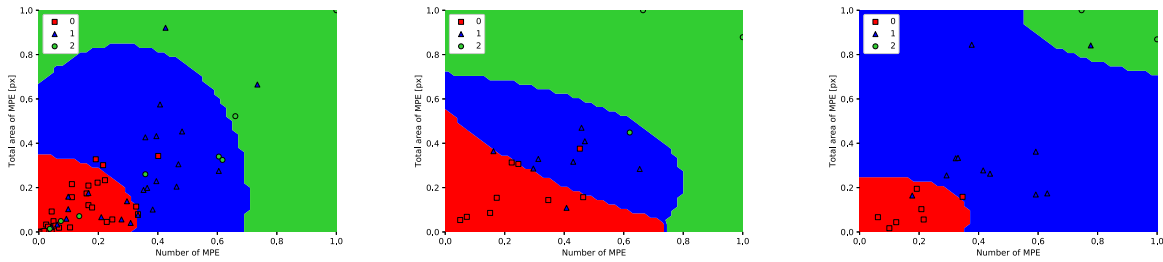


Figure 5.12: NB decision boundaries in the training, validation and test data sets (from left to right)

truth: \ predicted:	Class 0	Class 1	Class 2
Class 0	7	0	0
Class 1	2	7	2
Class 2	0	0	2

Table 5.7: RF confusion matrix for the training with the validation data set

5.2.6 Classification of MPE particles with Support Vector Machine

If a SVM used for classifying MPE particles into the three classes an accuracy of 80% was obtained for training with both the training and the validation data sets. Nevertheless, with a look at Figure 5.13 stands out that the decision domains are not representative of the data. In Table 5.10 and 5.9, the confusion matrices for training with the training and validation data sets are shown. As expected in case of the training with the training data set class 2 is not predicted anymore. The high accuracy was just obtained with the high number of correctly classified points of class 0 and class 1.

truth: \ predicted:	Class 0	Class 1	Class 2
Class 0	6	1	0
Class 1	1	8	2
Class 2	0	0	2

Table 5.8: RF confusion matrix for the training with the training data set

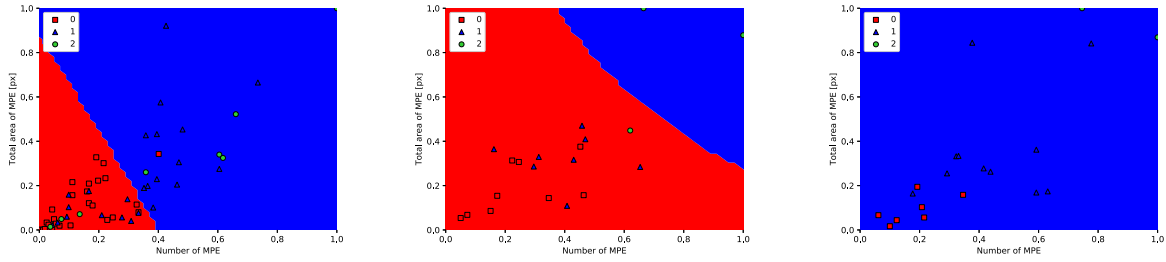


Figure 5.13: SVM decision boundaries in the training, validation and test data sets (from left to right)

truth: \ predicted:	Class 0	Class 1	Class 2
Class 0	7	0	0
Class 1	2	7	2
Class 2	0	0	2

Table 5.9: SVM confusion matrix for the training with the validation data set

5.2.7 Classification of MPE particles with Random Forest

The classification of MPE particles with a RF classifiers yielded an accuracy of 65 % for the training with the features of the training-set and an accuracy of 80 % for training with the data of the validation-set. In Figure 5.14, the decision domains are shown for the training-, validation- and test-set (from left to right). Compared with the decision made with a SVM, the classes are better chosen, but the class domains are separated. In Table 5.11 and 5.12, the confusion matrices are shown. In case of training with the validation data set the classes are mostly correctly classified. In case of training with the training data set the classes were often falsely predicted. Class 2 is chosen to rarely and class 0 and class 1 is chosen too often.

All in all similar accuracies were received with the above presented classifiers. Nevertheless with a look at the decisions made by the classifiers NB could convince with the best results.

truth: \ predicted:	Class 0	Class 1	Class 2
Class 0	6	1	0
Class 1	1	10	0
Class 2	0	2	0

Table 5.10: SVM confusion matrix for the training with the training data set

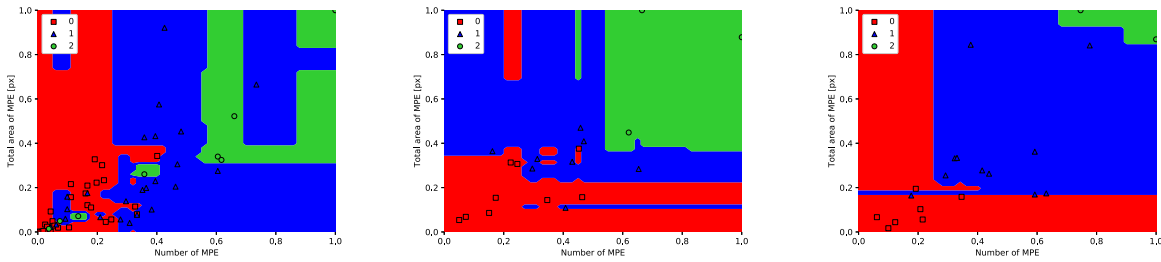


Figure 5.14: RF decision boundaries in the training, validation and test data sets (from left to right)

truth: \ predicted:	Class 0	Class 1	Class 2
Class 0	7	0	0
Class 1	2	7	2
Class 2	0	0	2

Table 5.11: RF confusion matrix for the training with the validation data set

5.3 Relationships between PE particles and CD3-positive immune/inflammatory response

In the following, it will be discussed in how far PE particles and especially the number of MPE particles, affect the strength of the occurring CD3-positive immune/inflammatory response.

First of all, the class numbers of the MPE particles per image are compared with the occurring strength of the CD3-positive immune response. In Figure 5.15, the three class numbers of the classes low, moderate and high immune/inflammatory response and the three class numbers (low, moderate and high) of the occurring strength of the MPE particles are compared. In 50 % the ground truth class numbers are equal, in 43 % the class numbers have a standard deviation of one and in the remaining 7 % the class numbers have a standard deviation of two.

If the MPE particles are not correlated to the CD3-positive immune/inflammatory response, a

truth: \ predicted:	Class 0	Class 1	Class 2
Class 0	5	2	0
Class 1	3	7	1
Class 2	0	1	1

Table 5.12: RF confusion matrix for the training with the training data set

much lower accuracy of about 33 %, corresponding to a random decision with three options, would be the case. Because of the higher accuracy of 50 %, a correlation between MPE particles and the occurring immune response can be assumed. In the next step the number of MPE particles

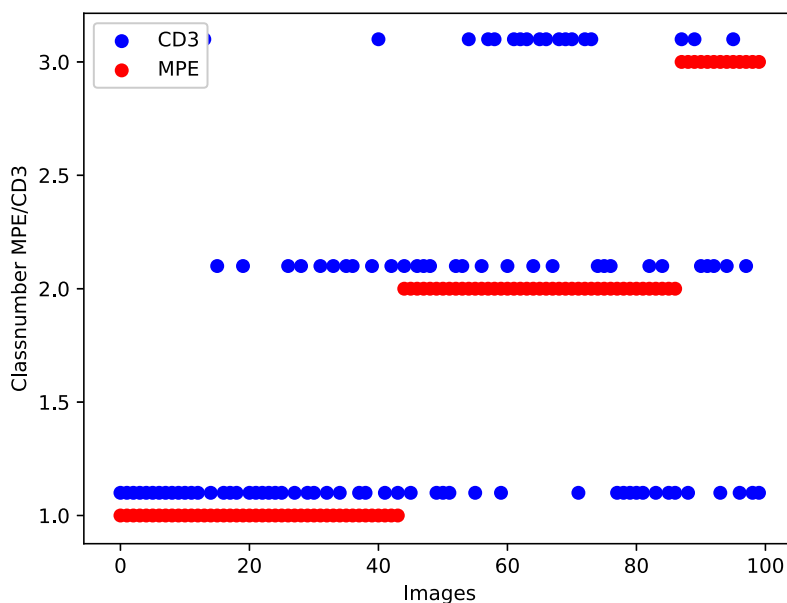


Figure 5.15: Relationship between MPE class numbers and CD3-positive class numbers for all images

and CD3-positive cells were compared. If a correlation exists, the number of CD3-positive cells should increase with the strength of the MPE particles. Therefore the MPE particles are sorted according to their size. In Figure 5.16 the graphical result for the training-, validation- and test-sets are shown separately. The blue lines correspond to the number of MPE particles, the red lines represent the number of CD3-positive cells. In order to recognize the course of the red line better, the results of a moving average filter of the number of the CD3-positive cells are included and presented as green line. In all three cases, the immune/inflammatory response is very noisy. The smoothed line of the moving average filter increases with the number of MPE particles first, but falls again in the last quarter. Generally, it is difficult to gather a tendency about the behavior of the CD3-positive cells due to the strong fluctuations. If the available data of the number of MPE particles and CD3-positive cells are mapped together in one image (see Figure 5.3) a similar behavior like in 5.16 occurs. For the left half of the graph, the CD3-positive cells seemed to correlate to the MPE particles. But with a look at the right side of the graph, the opposite occurs. The immune response is declining, the data should be not correlated anymore. It could be possible

5.3. RELATIONSHIPS BETWEEN PE PARTICLES AND CD3-POSITIVE IMMUNE/INFLAMMATORY RESPONSE

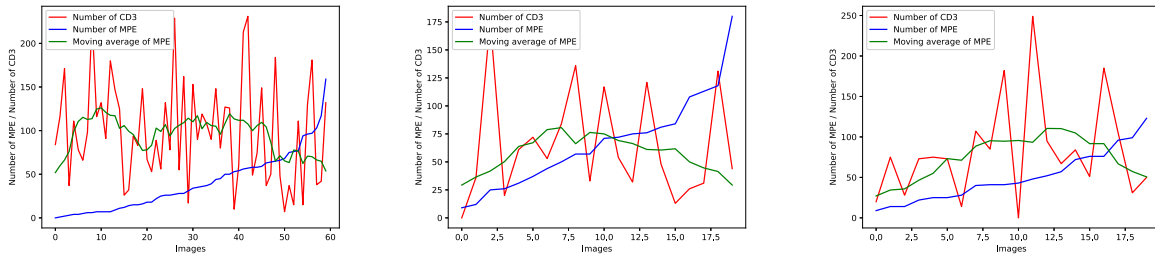


Figure 5.16: Relationship between MPE particles and CD3-positive cells for the training-, validation- and test-data

that, with a certain number of MPE, a saturation occurs. But, to be able to make precise statements, it is desirable to have more data.

In a third step the adjacent CD3-positive cells around the MPE particles and around the

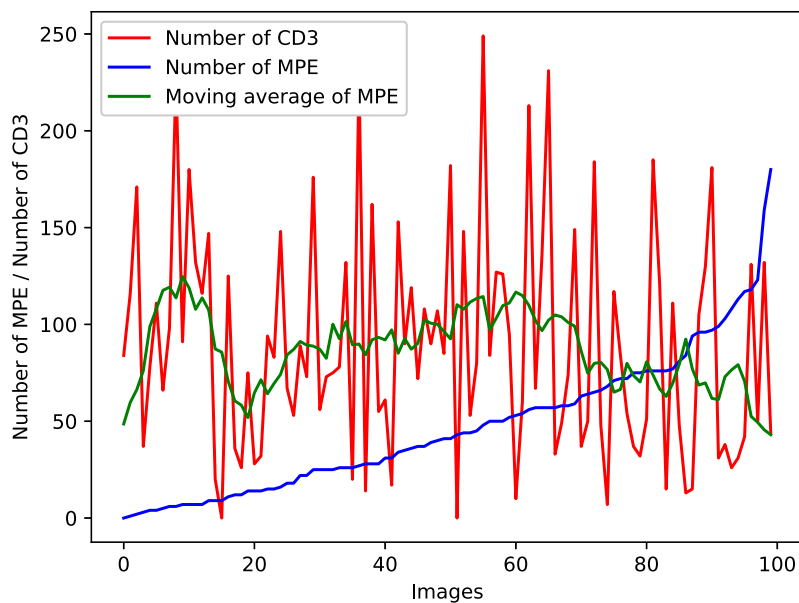


Figure 5.17: Relationship between MPE particles and CD3-positive cells for all Images

MacroPE/SMPE particles are counted for the test data set. In nearly all of the case CD3-positive cells, although a high or moderate CD3-positive immune/inflammatory response exists, were located around the MacroPE/SMPE. However, significantly more often CD3-positive cells were located next to MPE particles. In case of the test data set just one of the CD3-positive cells was

located next to the MacroPE/SMPE. In comparison to that, 31 CD3-positive cells were located around the MPE particles.

Chapter 6

Conclusion

Although the popular stain normalization methods are proven and successfully tested for the typically H&E stained colored images, it was possible to apply two of them, Macenko normalization and Reinhard normalization, to histological slice images, which were not colored with the typically H&E staining. Macenko normalization, followed by CD was suitable for the most images to improve the visibility of the available PE particles.

It could be also shown, that, with the Reinhard normalization, occurring variations in intensity and color within and in between the provided images disappeared completely. After a further CD it was possible to catch the CD3-positive cells with a fix threshold for all images.

With the assumption of a circular structure of the CD3-positive cells, it was possible to find them with the help of a circular blob detection method based on the difference of Gaussian, although they were overlapping. That is a strong improvement to available CD3-positive detection algorithms. Up to now, it was not possible to detect overlapping CD3-positive cells correctly (see CD3-Quantifier 2).

In Figure 6.1 the result of the preprocessing steps of the CD3-positive immune/inflammatory response is shown for a part of an image. The overlapping cells, e.g. in the upper left corner, were detected as single cells. Also good visible in the image is the advantage of the normalization and color deconvolution before thresholding. Thereby the dark occurring regions in the image, which are not CD3-positive cells, are not falsely detected as CD3-positive cells. Just with threshold method based on gray values this would be problematic. For the classification of the PE particles in MPE and MacroPE/SMPE, as well as the classification of the MPE particles and the CD3-positive cells into the three classes low, moderate and high, different supervised classification methods were tried. In all cases the simple classification method Naive Bayes receives the best results.

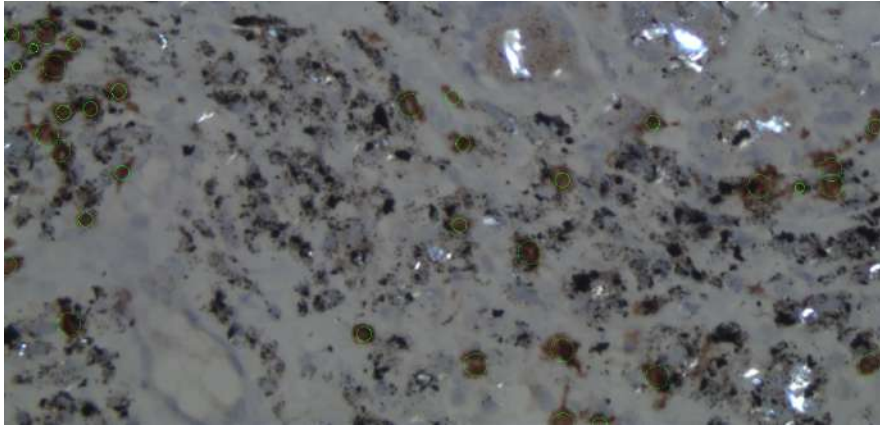


Figure 6.1: Circular blob detection of CD3-positive cells

All in all it can be summarized that the segmentation of the CD3-positive cells and the PE particles yielded mostly good results, nevertheless in few cases it was not possible to catch all MPE particles (see 4.2.2). For a more accurate segmentation it could be helpfully to use a target image, which is exactly provided for this special case of stain coloring.

The thesis, that the strength of the CD3-positive immune/inflammatory response increases with the number of occurring MPE particles could not be completely proven. Indeed with the help of the available data of 100 images it could be shown, that in 50 images the class number of the MPE particles corresponds to the class number of the occurring CD3-positive immune/inflammatory response, but nevertheless, with a comparison of the number of MPE to the number of CD3-positive cells it turned out, that the CD3-positive immune response increases with increasing MPE but false again from a certain point (see 5.3). Hopefully, with the help of the implemented GUI, the medical team can evaluate more images with a low time effort and reinforce the thesis.

Chapter 7

Summary

Aim of the thesis was the implementation of an automatic threshold based algorithm for the segmentation of histological slice images to reduce the time effort for the medical team required by a manual evaluation. The goal was to find a relationship between the aseptic loosening of hip and knee endoprosthesis and the occurring abrasion particles by establishing a relation between occurring micro-polyethylene (MPE) particles and the associated CD3-positive immune/inflammatory response response. A classifier for a similar problem had already been developed in 2015, however it failed at overlapping CD3-positive cells.

Generally, material abrasion is suspected to be an important aspect for the loosening process of endoprosthesis. The abrasion particles promote a formation of a synovial-like-interface-membrane (SLIM) between bone and endoprostheses, which leads to a loosening. About 5 % of the patients already experience primary complaints after 10 years. The endoprostheses have to be removed and replaced in a surgical procedure. Therefore it is of high importance to find the reasons for this failure in order to avoid such a surgical intervention which can be associated with considerable risks. In frame of this work, the polyethylene (PE) abrasion particles and the CD3-positive immune/inflammatory response was to be considered. In endoprosthetics, two different kinds of PE are used. A high molecular PE and lower particular PE. Higher cross-linked PE leads to mainly MPE particles and non-crosslinked PE to taller sized macro- and supramacro-polyethylene (MacroPE/SMPE). CD3-positive cells are considered as a measure for the occurring immune response. With different color reactions and techniques, it is possible to provoke the occurring CD3-positive cells and PE particles in the SLIM. PE particles are visible as bright regions and CD3-positive cells as small brown circular dots. A total of 100 images of 100 preparations of 52 patients were provided for this work. For the segmentation of the PE particles and CD3-positive cells, all steps of the pattern recognition pipeline for simple patterns were mandatory. In a first

step, different preprocessing methods had to be applied to obtain the specific information about the PE particles and the CD3-positive cells. In a further step the extracted features of the PE particles and the CD3-positive cells were used for the classification. Because of variations in color and brightness within and between the images, in a first step the images were normalized. It turned out that the two stain normalization algorithms by Macenko et al. and Reinhard et al. were suitable, although the images were not colored with the typically H&E staining. Both normalization methods are part of the stain normalization toolbox of Warwick. For a better visibility of the PE particles, Macenko normalization was used. With a linear per-channel normalization, it maps the calculated stain concentration matrix of the source image in optical density space to that of a target image. As a result, the images are more or less colored in an equal purple color and the PE particles are bright. With the linear normalization of Reinhard et al., it was possible to improve the visibility of the CD3-positive cells. The mean and standard deviations of the source images were mapped in LAB color space for each channel to the mean and standard deviations of the target image. As a result the color and intensity variation of the images disappeared and the CD3-positive cells were visible as brown dots. With a subsequent color deconvolution (CD) of the normalized images into three channels, corresponding to the stain saturation, the PE particles, especially the MPE particles, and the CD3-positive cells were clearly visible in most cases. Just in a few cases, in addition to the PE particles, some parts of the background were also visible as bright regions. With a simple binary thresholding, it was possible to catch the PE particles and the CD3-positive cells. In both cases a fixed threshold was suitable. As a result, the PE particles and the CD3-positive cells were visible as white regions on a black background. After that, the pictures were further preprocessed by eliminating white noise with a simple median filter and concluding holes between particles by morphological closing. After this step, it was possible to use a simple blob detection method for finding the contour, the area, the perimeters and the numbers of PE particles. For finding the midpoints, the number and the total area of the CD3-positive cells, a fast circular blob detection method based on the difference of Gaussian was used. With the assumption that CD3-positive cells had to be circular, it was possible to catch singular CD3-positive cells of overlapping CD3-positive cells and clusters. The extracted features, containing information about PE particles and CD3-positive cells, were used for training and evaluating the three different supervised classifiers naive Bayes (NB), support vector machine (SVM) and random forest (RF). NB is an often used simple classification algorithm with a mostly good performance. It is similar to a Bayesian classifier but with the simplification assumption of the independence between features. SVM is a linear classifier for separating the different classes with the help of the closest points of each class. RF is a method relying on the combination

of many weak learners. In addition to these three classifiers, a nearest neighbor classifier was implemented for counting the numbers of CD3-positive cells adjacent to the MacroPE/SMPE and MPE particles. For an easy handling, the methods introduced above were included into a graphical user interface (GUI) for counting the number of CD3-positive cells, MacroPE/SMPE and MPE particles and for calculating the number of adjacent cells to the MPE and MacroPE/SMPE particles.

In general it turned out that the two features total number of CD3-positive cells and number of CD3-positive cells per image were suitable for separating the immune/inflammatory response into the three classes low, moderate and high. For separating the PE particles into MacroPE/SMPE and MPE, the perimeters and areas of each particle per image were suitable. In a further classification, the MPE particles were separated into the three classes low, moderate and high with the help of the number and the total area of MPE per image. For the classification, the available information about the 100 images was separated into three data sets: 60 images for training, 20 images for validation, and 20 images for testing. The classification problem of the CD3-positive immune/inflammatory response with NB and RF achieved an accuracy of 80 % for training with the training data set and an accuracy of 70 % for the validation data set. Using SVM, a similar but slightly worse accuracy of 70 % could be obtained with both the training and the validation data sets. With a look at the decision domain, it becomes obvious that the NB classifier separated the classes with the best performance. For separating the PE particles into MacroPE/SMPE and MPE and counting the MacroPE/SMPE particles per image, a NB classifier were used. Based on the training data set the number of MacroPE/SMPE particles could be achieved with an accuracy of 55 %. A standard deviation of 1 increased the accuracy to 90 %. Based on the validation data set, the number of MacroPE/SMPE particles were predicted with an accuracy of 60 %, an increasing standard deviation of 1 led to an accuracy of 85 %. In both cases a standard deviation of 2 led to an accuracy of 95 %. The classification of the MPE particles with NB and SVM led to a similar accuracy of 80 % for both the training with the training and validation data set. RF achieved an equal accuracy of 80 % for training with the validation data set, but a worse accuracy of 65 % for the training with the training data set. All in all, with a look at the decision domains, it turned out that NB had the best performance. To proof the thesis, whether an increasing number of MPE particles correlates to the strength of the CD3-positive immune/inflammatory response in a first step the class numbers of the MPE particles and CD3-positive cells were compared. In 50 % of the cases the class numbers were equal, which implies correlation, as, in case of a random decision, a much lower accuracy of about 33 % would be the case. In addition CD3-positive cells were located around MPE in a significantly higher frequency than around MacroPE/SMPE. Nevertheless, the

immune/inflammatory response increases with increasing MPE but false again from a certain point. To make precise statements about the relationship between MPE particles and the CD3-positive cells it is desirable to have more data. Hopefully, the thesis can be reinforced with a low time effort for the medical team by evaluating more images with the help of the implemented graphical user interface.

List of Figures

2.1	CD13-Quantifier for a histopathological slice image [Hop16]	3
3.1	SLIM consensus classification of joint prosthesis pathology [Hop17]	5
3.2	Particle algorithm [Kre16]	6
3.3	Number of hip and knee implants in Germany [Lie16]	7
3.4	Left: Hip endoprosthesis with Me-PE sliding pairing; Right: Artificial knee endoprosthesis [Hop16]	8
3.5	Different material combinations for the sliding pair, from left to right: 1. metall-metall, 2. ceramics-ceramics, 3. ceramics-polyethylene, 4.metall-polyethylene [Hop16]	8
3.6	Aseptic loosening of a hip endoprosthesis; Formation of a SLIM (blue arrow) [Hop16]	9
3.7	Histological images with a low, moderate and high CD3-positive immune/inflammatory response (from left to right)	9
3.8	Histological image with SMPE (yellow arrow), MacroPE (red arrow) and MPE (blue arrow)	10
4.1	Pattern recognition pipeline for simple patterns [Pau98]	14
4.2	Preprocessing	14
4.3	Different histopathological images with a high variation in color and brightness . .	15
4.4	Macenko normalized histopathological images with a high color and intensity variation	16
4.5	Chosen target image for Macenko Normalization [ToW15]	17
4.6	Reinhard normalized histopathological images	19
4.7	Chosen target image for Reinhard normalization [Mag09]	19
4.8	Color deconvolution of Macenko normalized images	21
4.9	Color Deconvolution of the original images	22

4.10	Color Deconvolution of Reinhard normalized images [Kha14]	23
4.11	Top: Binary thresholding of the second channel of the Macenko normalized color deconvolved images for finding the PE particles; Botton: Binary thresholding of the second channel of the Reinhard normalized color deconvolved images for finding the CD3-positive cells	24
4.12	Structure element	26
4.13	Top: Closing followed by a small median filter for finding PE particles; Bottom: Median filter for reducing white noise for finding CD3-positive cells	26
4.14	Top: Blob detection for finding PE particles; Bottom: Circular blob detection of the CD3-positive cells	28
4.15	Preprocessing Pipeline	28
4.16	Distance Measure: blue object represents a PE particle, yellow object: represents one CD3-positive cell; the black line represents the minimal calculated distance between the contour of the PE particle and the midpoint of the CD3-positive cell	32
4.17	Graphical User Interface	33
4.18	Graphical User Interface with the evaluation for a single image	34
5.1	Features of CD3-positive immune/inflammatory response	36
5.2	Left: CD3 features for training-set; middle: CD3 features for validation-set; right: CD3 features for all test datat	36
5.3	Features of PE particles	37
5.4	Left: PE features for trainingsset; middle: PE features for validationset; right: PE features for testset	38
5.5	PE particle distribution for the features area and perimeter for two images	38
5.6	MPE features for training-, validation- and test-set (from left to right)	39
5.7	NB decision boundaries in the training, validation and test data sets (from left to right)	39
5.8	SVM decision boundaries in the training, validation and test data sets (from left to right)	41
5.9	RF confusion matrix for the training with the validation data set	42
5.10	NB decision boundaries in the training, validation and test data sets (from left to right)	43
5.11	Groundtruth number of MacroPE/SMPE particles of Testdata versus predicted number of MacroPE/SMPE for training (left side) and validation data set (right side) with NB	44

5.12 NB decision boundaries in the training, validation and test data sets (from left to right) 45

5.13 SVM decision boundaries in the training, validation and test data sets (from left to right) 46

5.14 RF decision boundaries in the training, validation and test data sets (from left to right) 47

5.15 Relationship between MPE class numbers and CD3-positive class numbers for all images 48

5.16 Relationship between MPE particles and CD3-positive cells for the training-, validation- and test-data 49

5.17 Relationship between MPE particles and CD3-positive cells for all Images 49

6.1 Circular blob detection of CD3-positive cells 52

List of Tables

5.1	NB confusion matrix for training with the validation data set	40
5.2	NB confusion matrix for training with the training data set	40
5.3	SVM confusion matrix for training with the validation data set	41
5.4	SVM confusion matrix for the training with the training data set	42
5.5	RF confusion matrix for the training with the training data set	42
5.6	RF confusion matrix for the training with the validation data set	43
5.7	RF confusion matrix for the training with the validation data set	45
5.8	RF confusion matrix for the training with the training data set	45
5.9	SVM confusion matrix for the training with the validation data set	46
5.10	SVM confusion matrix for the training with the training data set	46
5.11	RF confusion matrix for the training with the validation data set	47
5.12	RF confusion matrix for the training with the training data set	47

Bibliography

- [Bis06] Christopher M Bishop. *Pattern recognition and machine learning*. springer, 2006.
- [Cri13] Antonio Criminisi and Jamie Shotton. *Decision forests for computer vision and medical image analysis*. Springer Science & Business Media, 2013.
- [Dou92] Edward Dougherty. *Mathematical morphology in image processing*. CRC press, 1992.
- [Gho14] Dibyendu Ghoshal and Pinaki Pratim Acharjya. Image segmentation by mathematical morphology: An approach through linear, bilinear and conformal transformation. *World Academy of Science, Engineering and Technology, International Journal of Mathematical, Computational, Physical, Electrical and Computer Engineering*, 8(8):1138–1141, 2014.
- [Hop16] Felix Hopf. *Materialabhängige CD3-Response in der SLIM bei dysfunktionalen Gelenkendoprothesen*. PhD thesis, Freie Universität Berlin, 2016.
- [Hop17] Felix Hopf, Peter Thomas, Stefan Sesselmann, Marc N Thomsen, Maximilian Hopf, Johannes Hopf, Manfred G Krukemeyer, Herbert Resch, and Veit Krenn. Cd3+ lymphocytosis in the peri-implant membrane of 222 loosened joint endoprotheses depends on the tribological pairing. *Acta Orthopaedica*, pages 1–7, 2017.
- [Kha14] Adnan Mujahid Khan, Nasir Rajpoot, Darren Treanor, and Derek Magee. A nonlinear mapping approach to stain normalization in digital histopathology images using image-specific color deconvolution. *IEEE Transactions on Biomedical Engineering*, 61(6):1729–1738, 2014.
- [Köl15] B Kölbl, S Wienert, J Dimitriadis, D Kendoff, T Gehrke, M Huber, L Frommelt, A Tiemann, K Saeger, and V Krenn. Cd15-fokus-score zur diagnostik der periprothetischen gelenkinfektion. *Zeitschrift für Rheumatologie*, 74(7):622–630, 2015.

- [Kre16] V Krenn, F Hopf, P Thomas, M Thomsen, S Usbeck, F Boettner, S Müller, D Saberi, T Hügle, M Huber, et al. Supramakropartikuläres polyethylen bei entzündungen periprothetischer membranen. *Der Orthopäde*, 45(3):256–265, 2016.
- [Lie16] Thoralf Randolph Liebs. Eprd-jahresbericht 2015, 2016.
- [Lin98] Tony Lindeberg. Feature detection with automatic scale selection. *International journal of computer vision*, 30(2):79–116, 1998.
- [Low04] David G Lowe. Distinctive image features from scale-invariant keypoints. *International journal of computer vision*, 60(2):91–110, 2004.
- [Mac09] Marc Macenko, Marc Niethammer, JS Marron, David Borland, John T Woosley, Xiaojun Guan, Charles Schmitt, and Nancy E Thomas. A method for normalizing histology slides for quantitative analysis. In *Biomedical Imaging: From Nano to Macro, 2009. ISBI'09. IEEE International Symposium on*, pages 1107–1110. IEEE, 2009.
- [Mag09] Derek Magee, Darren Treanor, Doreen Crellin, Mike Shires, Katherine Smith, Kevin Mohee, and Philip Quirke. Colour normalisation in digital histopathology images. In *Proc Optical Tissue Image analysis in Microscopy, Histopathology and Endoscopy (MICCAI Workshop)*, volume 100. Daniel Elson, 2009.
- [Mül15] M Müller, G Wassilew, and C Perka. Diagnostik und behandlung von abrieberkrankungen in der hüftendoprothetik. *Zeitschrift für Orthopädie und Unfallchirurgie*, 153(02):213–229, 2015.
- [Nö15] Elmar Nöth. Pattern recognition (pr). University of Erlangen-Nuremberg, 2014/15.
- [Pau98] Dietrich WR Paulus and Joachim Hornegger. *Applied pattern recognition: A practical introduction to image and speech processing in C++*. Morgan Kaufmann Publishers, 1998.
- [Rei01] Erik Reinhard, Michael Adhikhmin, Bruce Gooch, and Peter Shirley. Color transfer between images. *IEEE Computer graphics and applications*, 21(5):34–41, 2001.
- [Ron06] Christian Ronse, Laurent Najman, and Etienne Decencière. *Mathematical morphology: 40 years on: proceedings of the 7th International Symposium on Mathematical Morphology, April 18-20, 2005*, volume 30. Springer Science & Business Media, 2006.

- [Rui01] Arnout C Ruifrok, Dennis A Johnston, et al. Quantification of histochemical staining by color deconvolution. *Analytical and quantitative cytology and histology*, 23(4):291–299, 2001.
- [Tea] Scikit-Image Development Team. Morphological filtering. http://scikit-image.org/docs/dev/auto_examples/xx_applications/plot_morphology.html. [Accessed 2017-09-17].
- [Tea17a] Opencv Dev Team. Structural analysis and shape descriptors. http://docs.opencv.org/2.4/modules/imgproc/doc/structural_analysis_and_shape_descriptors.html, 2017. [Accessed 2017-09-15].
- [Tea17b] Scikit-Image Development Team. Blob detection. http://scikit-image.org/docs/dev/auto_examples/features_detection/plot_blob.html, 2017. [Accessed 2017-09-17].
- [ToW15] Stain normalisation toolbox of warwick. <http://www2.warwick.ac.uk/fac/sci/dcs/research/tia/software/sntoolbox/>, 2015. [Accessed 2017-09-15].
- [Vis17] Doxygen Open Source Computer Vision. Contours : Getting started. http://docs.opencv.org/trunk/d4/d73/tutorial_py_contours_begin.html, 2017. [Accessed 2017-09-15].